

# Geophysical studies to delineate groundwater aquifer in arid regions: A case study, Gara Oasis, Egypt

Mohamed NAZIH<sup>1</sup> , Mohamed GOBASHY<sup>1,\*</sup> , Sultan ARAFFA<sup>2</sup> ,  
Khaled Soliman SOLIMAN<sup>1</sup> , Ahmed ABDELHALIM<sup>3</sup> 

<sup>1</sup> Cairo university, Faculty of Science, Geophysics Department, Giza, Egypt;  
e-mails: mohamednazih736@yahoo.com, gobashy@sci.cu.edu.eg,  
khaled\_soliman2005@yahoo.com

<sup>2</sup> National Research Institute of Astronomy and Geophysics (NRIAG), Helwan, Egypt;  
e-mail: sultan\_awad@yahoo.com

<sup>3</sup> Cairo University, Faculty of Science, Geology department, Giza, Egypt;  
e-mail: ahmedabdelhalim@cu.edu.eg

**Abstract:** Groundwater is an important factor in establishing new urban communities, especially in coastal arid and semi-arid regions. Egypt is one of the world's driest countries, with hyper-arid territory accounting for 86% of the total area and arid and semi-arid terrain accounting for the rest. The present work aims to demonstrate the powerful integration of geophysical techniques to assess groundwater potentiality and suitability in Gara Oasis (GO), which describes a good example of Egypt's strategic southern extension of its arid north-western coast. Geophysical methods, including electrical resistivity and aeromagnetics, were used to evaluate groundwater resources. The study region reduced to pole total magnetic intensity map is subjected to digital filters that include derivatives, analytic signal, and tilt angle. The possible structures controlling the shallow and deep aquifers are delineated and integrated with geoelectric results. Moreover, two magnetic tomography sections are constructed to show the subsurface distribution of magnetic susceptibilities and formation boundaries. Ten vertical electric soundings (VESs) are measured and used in this study to construct four geoelectrical cross-sections. According to the results, Gara's commonly calculated subsurface resistivity model comprises six major resistivity layers. The 5th layer, in particular, is composed of Fractured dolomitic Limestone and represents a possible promising shallow aquifer. Moreover, as evidenced by various magnetic data filters, the shallow (Miocene carbonate) and deep (Nubian sandstone) aquifers are structurally controlled and regulated by a system of faults or contacts. These contacts trends NW–SE, E–W, and NE–SW as common trends emerged from the total derivative and tilt maps. Results suggest that the central part (N–S zone) together with the western side of Gara, have the most notable aquifer possibility demanded future improvement strategies.

**Key words:** Gara Oasis, arid regions, geoelectric, magnetic, groundwater aquifer

\*corresponding author, e-mail: gobashy@sci.cu.edu.eg

## 1. Introduction

North Africa's great Sahara is one of the driest lands on the earth. The great African Sahara extends from Egypt at the east to Morocco at the west. It measures approximately 4800 km from east to west and between 1287 km and 1931 km from north to south. Water represents the critical factor of life in this hyper-arid region. Due to the scarcity of rainwater, groundwater is the main source of water. The search and assessment of the groundwater are of utmost importance in these regions. Many investigations have been tried for groundwater exploration using various geophysical methods due to their efficiency and reliability such as the electrical resistivity, magnetic and electromagnetic methods. Such studies have inspected the relationship between geomorphology, tectonic structures, and groundwater (Gobashy and Al-Garni, 2008; Al-Garni and Gobashy, 2010; Apaydin, 2010; Manning, 2011; Yuan et al., 2011; Herrera and Garfias, 2013; Roques et al., 2014; Arnous et al., 2017; El Rayes et al., 2017; Abdelazeem et al., 2020). These studies confirmed that faults and folds greatly affect the groundwater flow regime.

On the other hand, groundwater is influenced via geological and anthropogenic impacts. The mineralogy of rock categories, geological structures, water recharge source, period of occupancy, and aquifer conditions are all geological impacts. Anthropogenic impacts include population growth, over-pumping, and agricultural and industrial development without appropriate corrective procedures (Chapman, 1996). When water flows from recharge to discharge regions, it exhibits significant changes in groundwater chemistry according to many factors including precipitation, weathering, dissolution of minerals, evaporation, topography, exchange of ions, and saltwater interference (Elango and Kannan, 2007; El Osta et al., 2021). The interaction of groundwater to saline water with the host rock can alter the chemistry of the groundwater to irrigate its validity. Groundwater is recharged by vertically infiltrating rainwater, the influence of host rocks is more evident (Abdelazeem et al., 2020).

The present geophysical and geological study is carried out on the Gara Oasis (GO), which is one of the many oases that are distributed all over the Sahara and one of the main seven depressions in the Egyptian desert that represent typical arid regions. It is one of Egypt's most private destina-

tions and is considered an excellent example of the virgin oasis of main natural depressions in Egypt's Western Desert (WD) and the great African Sahara.

Many studies were applied basically for evaluating and delineating the groundwater resources and implement a complete evaluation of the quality concerning groundwater using joint geophysical and geological methods within this region and other close regions of similar conditions, among them (*Said, 1962 & 1990; Gindy and El Askary, 1969; Himida, 1970; El Shazly et al., 1976; Abdel-Mogheeth et al., 1996; Awad et al., 1995; Aly, 2001 & 2007; Rabeh, 2004; Aly et al., 2008 & 2011; Abo EL-Fadl et al., 2015; El Hossary, 2013; Hedia, 2015; Khalil et al., 2015; Aly, 2015; Aly et al., 2016; Farrag et al., 2016; Saleh et al., 2016; Farrag and Sediek, 2017; Salman et al., 2018; Gad et al., 2018; Abdel Zaher et al., 2018; Aly, 2020; Moghazy and Kaluarachchi, 2020; Abdel-Gawad et al., 2020*). While particularly for Gara, a relatively few studies are carried out (*Aly, 2015*). Geoelectrical investigation comprising VES (Vertical electrical sounding) is a powerful method for the evaluation of aquifer qualities. These studies constitute the base for planning underground water wells and the future development of the aquifer. Magnetic methods, on the other hand, support these VESs results by delineating the structural controls of this aquifer. Hence, improving a relevant groundwater sustainability expansion system is essential to minimize the consequences of irregular good excavation and over-abstraction of groundwater (*El Osta et al., 2020 & 2021; Masoud, 2020; El Osta, 2018*).

This study is aimed to investigate and delineate the shallow Miocene groundwater aquifer with changes in the GO's vertical and lateral facies. This is accomplished for the first time in GO to the knowledge of the authors. The study is intended to facilitate the conservation and sustainability of the groundwater through the integrated interpretation of Electric and magnetic measurements in the area. The aeromagnetic data is integrated with the geoelectrical method to delineate the subsurface structure of the area. Moreover, a road map for constructing groundwater wells in the targeted area is developed. The results should be useful to regulate the oasis' underground water resources to limit the decline in levels and quality of groundwater in the region and to support future improvements within the region.

## 2. Study area and methods

### Overview of the study area

Gara Oasis is located between Siwa Oasis (SO) (depression) in the north-eastern part (between Siwa Oasis and Marsa Matrouh) and the north-western part of Qattara depression within latitudes  $29.575^{\circ}$  and  $29.675^{\circ}$  N and longitudes  $26.475^{\circ}$  and  $26.55^{\circ}$  E (Fig. 1). Gara includes thermal sources (hot springs) and wells. The GO lies around 40 m below sea level in a depression (Aly, 2015). The Gara depression, located in Egypt's north-western corner, and the closest depression to Siwa Oasis (SO), is considered as one of the desert areas that have no running canals or streams. GO is essentially dependent on groundwater, in particular, brackish water that flows from the limestone fractured Miocene aquifer (shallow), distinguished as the source for farming of agricultural, manufacturing, and constructive improvement in the region (El Hossary, 2013; Abo EL-Fadl et al., 2015; Aly, 2015; Gad et al., 2018; Aly, 2020). Owing to the availability of groundwater that may

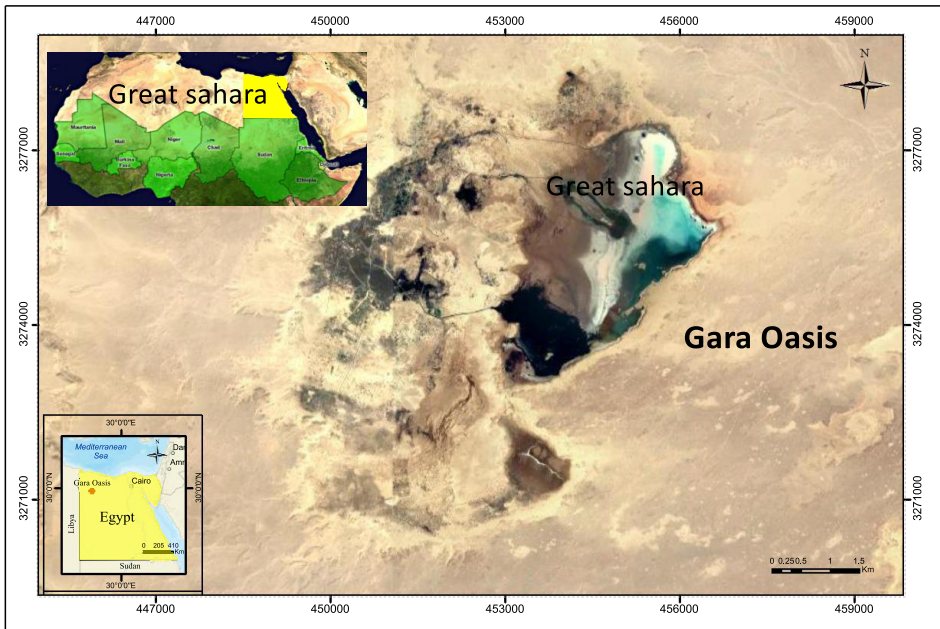


Fig. 1. Location map of the study area, Gara Oasis, North-Western Desert, Egypt.

be employed for future development, depression attracted significant attention in earlier studies. It has saline lakes developed because of the lack of sufficient drainage (*Moghazy and Kaluarachchi, 2020*).

GO groundwater is a very significant natural resource for the people of these oases because of the arid environment of Northern Africa and the great Sahara (*Aly et al., 2011; Nazih et al., 2022*). It is artesian and available from both the deep aquifers of Nubian sandstone (NSSA) and shallow Eocene and Miocene carbonate aquifers of the Tertiary carbonate (TCA) in natural springs, and drilled wells (*El Hossary, 2013*). Many wells have been drilled to correspond to the expansion of the agricultural land, development projects, and food industry (*Salheen, 2013*). Since the main activity in GO, in particular, is agriculture, consequently, aquifer thickness, hydro-geochemical characteristics, and quality are fundamentally determined for evaluating and improving groundwater aquifers and their operation to manage the agriculture of these aquifers (*El Osta et al., 2021*) and other similar regions of the same geological conditions.

### **Climatic conditions**

According to *Abdallah (2007)*, the lowest recorded air temperature in January is about  $5.80^{\circ}\text{C}$  and in July is  $37.8^{\circ}\text{C}$ . The diurnal range is  $32^{\circ}\text{C}$ . Precipitation is precarious and variable  $0.87\text{ mm/month}$  and evaporation ranges between  $4.8$  to  $13.5\text{ mm/day}$ . Contemporaneously, air temperature records its maximum value and rainfall drops to nothing ceases to excess and consequently evaporation becomes extreme and responsible for the formation of the salty layer in the soil profile with a marked decrease in sub-soil water level. The main wind direction in the area is NE, SE, and NW with general rations of  $12.4\%$ ,  $18.2\%$ , and  $24.4\%$ , respectively. The physical effects of this wind (erosion and deflation) attain their highest effect in April. The transported fine sand and salt fragments are deposited in low lands within and around the oasis. This phenomenon affects the impermeable layer by soil erosion carrying the soil matrix away leading to a decrease in the soil profile and thus raising the groundwater table. Based on the above, insufficient rainfall, high temperature, and high evaporation and aspiration, increase the capillary rise of water to the sediments on the surface bringing about a concentration of salt crystals in the soil surface causing the increasing acceleration of salt weathering activities.

### Geomorphological setting

Geomorphologically, the Gara depression was initiated as a result of the folding followed by faulting and erosional effect, the location of the oasis in the western desert’s northern portion made the depression a natural discharging locality for the different aquifers through springs and wells (*Abdel-Gawad et al., 2020*). The surface of the depression and its surroundings represents the following geomorphological units (Figs. 2 and 3): sabkha deposits, lake, the Moghra Fm, Mokattam group, and Marmarica Fm. Quaternary sediments of a thickness of 0.5 to 3 m, comprising aeolian and alluvial sediments displaced by sabkhas or salt near the lake’s vicinity, were evident in the investigated region (*Gad et al., 2018*). The composite stratigraphic section in and about the Gara depression (Fig. 4) reveals that the basement of the Precambrian complex consists of gneiss and volcanic sedimentary sequences and granitoid in the southern section related to Arab-Nubian Shield Massif and to the north, there is a Phanerozoic sedimentary succession (*Abouelmagd et al., 2014*).

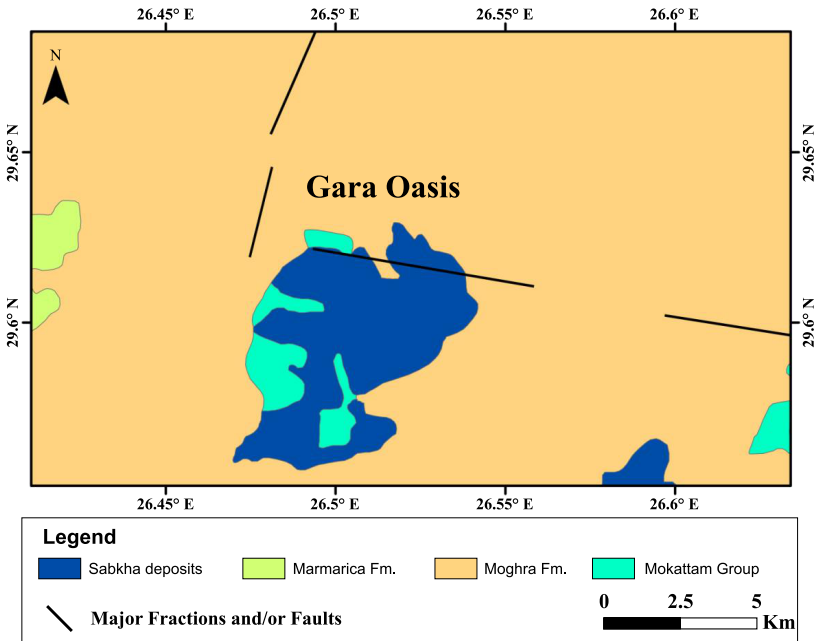


Fig. 2. Geological and Geomorphological map of the important features developed in Gara Oasis area, Egypt (modified after *Conoco, 1987*).

## Surface and underground water

Within the GO, the hydrogeological layers are ranged from 450 to 600 m thick of the fractured dolomitic limestone (shallow Miocene and Eocene aquifer) overlying the Nubian sandstone aquifer (NSSA, deep aquifer). Shale and clay layers with low permeability separate the fractured Miocene-Eocene carbonate zones from the underlying NSSA. The Nubian aquifer NSSA is about 2600 meters thick and belongs to the Paleozoic and Mesozoic periods. The upper zone is approximately 500 meters in thickness and is saturated with freshwater including less than 500 ppm (mg/l) salinity and around 70°C temperature (Abo EL-Fadl *et al.*, 2015). In the north and west, the residual sand thickness is reduced. The heads of water pressure of the aquifer's Nubian sandstone vary from 80 m in the west of Gara and Siwa districts, where springs and shallow wells occur, to 120 m in the east (El Arabi *et al.*, 2013; Abo EL-Fadl *et al.*, 2015; GPC, 1991). The salinity ranges from 1600 to 8000 ppm of water from shallow wells in the shallow Miocene aquifer, while the salinity ranges from 300 to 400 ppm from deep artesian wells (NSSA, Nubian sandstone aquifer) (Aly, 2001).

### 2.1. The general geological setting

To define the hydrogeological conditions of the GO, the geologic setting of the oasis should be reviewed. It will be discussed under two topics, the lithostratigraphy, and structural setting (Figs. 2 and 3):

#### a) The lithostratigraphy

The outcropping formations (surface geology) and the subsurface formations, which are related to groundwater as water-bearing formations in the Gara area, include various rock units. These units cover geological ages between Cambrian and quaternary ages. This succession had underlain by granitic rocks. The Phanerozoic rocks of the GO area and its environments are discussed in the following:

#### Surface stratigraphy

The oasis's surface geology is characterized and identified by sabkhas, which are quaternary deposits of silt, evaporated deposition, and clay combinations (Figs. 3a and b). The Mokkatam group of Middle Eocene (white calcareous limestone associated with grey shale and evaporite layers) is among

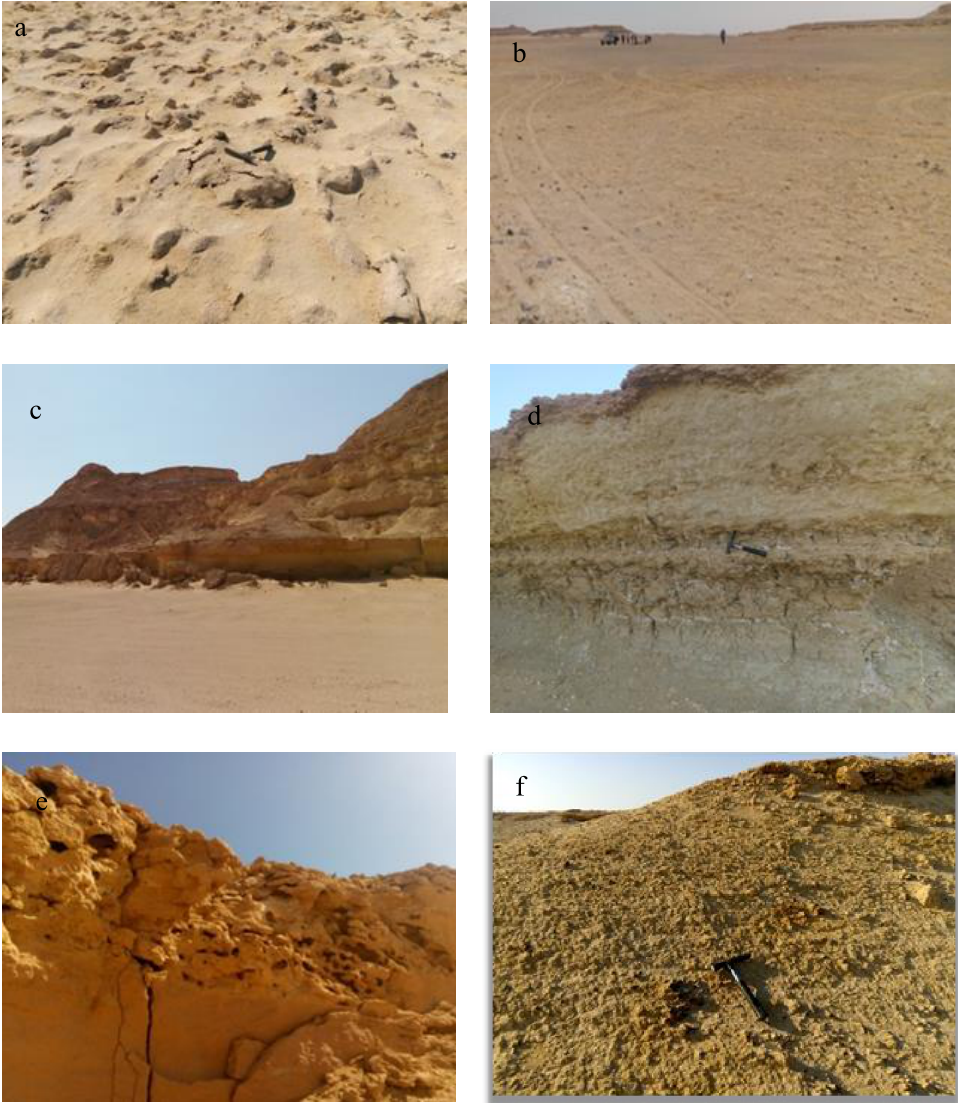


Fig. 3. Surface geological formations in the study area: (a) salt sabkha (Karshef), (b) quaternary deposits, (c) upper carbonate unit of Eocene, (d) lower shale unit of Middle Eocene, (e) karst features at most upper Eocene limestone and (f) glauconitic sand with iron oxides concretions at Naqb Al-Ahmer.

the oldest rocks in the area and is exposed in the southeast and west section of the region. There are many erosional drainage lines inside, and throughout, the northern escarpment surrounding the depression, largely impacted by the developing trends of fracture systems in NW–SE and NE–SW. The Middle Eocene chalky limestone Mokkatam Group is exposed with an unwrapped thickness of 75 m has been measured (*Antar, 2011*). This section consists of an upper unit of white chalky limestone and a lower shale unit 22 m thick which dominated glauconitic sand and siltstones with iron oxides concretions (Fig. 3f). The later shale unit observed west Ain Timeira and formed Naqb Al-Ahmer due to SW of Gara depression.

Era	Age	Log	Average Thickness	Lithic description	Depositional environment
Cenozoic	Tertiary		250 m	Limestone with marl (Marmarica Fm.) Sandstone, siltstone, shale (Moghra Fm.)	Shallow marine Fluvio-Marine
	Eocene		350 m	Limestone intercalated with shale, marl, evaporites beds (Mokattam Gr.)	Shallow marine
Mesozoic	Cretaceous		600 m	Sandstone with shale and carbonate intercalations (L. Cretaceous), overlain by impermeable layer of carbonaceous shale and argillaceous limestone (U. Cretaceous)	Shallow marine, near shore
Paleozoic	Carboniferous		912 m	Sandstone with shale and limestone	Near shore, Continental
	Devonian		347 m	Mudstone, siltstone, carbonaceous sandstone, limestone & dolomite	Fluviatile, Continental, Shallow marine
	Silurian		626 m	Mudstone and siltstone (Kohla Fm.)	Fluviatile, Marine
	Ordovician/Cambrian		315 m	Sandstone intercalated with shale and siltstone beds	Continental
Pre-Cambrian			?	Basement complex, Granite, Gneisses	

Fig. 4. Composite stratigraphic section in Gara depression and its surroundings (oases) formations, Egypt (compiled after *Abdel-Gawad et al., 2020; Afifi, 2005; EGPC, 1992; Ibrahim, 1991*).

Moreover, this Middle-Eocene unit is overlain by silicified wood and quartzitic gravel of Lower Miocene Moghra Formation (Moghra Formation, consisting of a continuous to shallow marine silici-clastic succession with an abundance of silicic wood, including shale, siltstone, and white sandy carbonate layers) (Fig. 3d). In the subsurface, the Formation of Moghra, a clastic series of fluvio-marine Early Miocene delta basins that laterally grade marine facies (*Said, 1990*), the Upper Eocene overlying by uncon-

formable. In this particular region of the depression, the Middle Miocene of the Marmarica Formation about (94 m thick) provides a more comprehensive portion of the area of research (Figs. 3c & f). It consists mostly of calcareous limestone, dolomite, and shale (Upper Miocene, Marmarica Formation consisting of grayish-white calcarenite, with little shale association including fossil-rich white limestone). The north scarp of the depressions Gara and Siwa oases, and various hills in Mortazak, Gebel El Dakrour, Zomaq, Khameisa, and El Mawta, are fundamentally produced. It is 78 m high. The thickness of the surface is 78 m at the scarp and 94 m throughout the whole depression (*Gindy and El Askary, 1969*).

The Quaternary deposits are expressed in the Gara Oasis by alluvium and aeolian deposits cover Tertiary rocks (Fig. 3b). The quaternary deposits have a thickness range from 2 m to 3 m soil zone which at the lakes approach is replaced with salt or sabkha (*Gad et al., 2018*). The area nearby the lake composes salt crust (Korsheef) or sabkha (Fig. 3a).

### **Subsurface stratigraphy**

A Paleozoic, Mesozoic, and Cenozoic succession with a thickness of about 3400 m makes up the stratigraphic subsurface sequence (*El Hossary, 1999*).

There are two major clastic and carbonate deposition cycles (periods) in it (*Abdel-Gawad et al., 2020*) (Figs. 2 and 4). The Paleozoic and Mesozoic groups are represented in this primary clastic cycle, which involves the oldest sedimentary strata. The Tertiary Eocene and Miocene groups are part of the other cycle of carbonate facies. The whole Paleozoic, Mesozoic, and Cenozoic stratigraphic succession were controlled by several normal faults orientated northwest–southeast (NW–SE), east–west, northeast–southwest (NE–SW), and north–south, that stabilized at the top of the basement (*Said, 1962; Afifi, 2005*). The development of the Gara and Siwa springs is caused by certain faults (*Shata, 1982*) and the lithofacies variation and thicknesses of formation.

### **b) The structural setting**

The GO occupies a regional synclinal fold trend (NNW–SSE), which is associated with the end of the Eocene period, and the compressional Oligocene forces (NW–SE) has influenced Cretaceous folding which has led to the creation of the “Syrian Arc System” while in a NE–SW trend characterized by normal and reverses faulting parallel to the axes of the fold. (*Kaiser and*

*Vollen Weider, 1972*). The study area shows also the major structural characteristics mainly those, which extend in northwest–southeast (NW–SE) and northeast–southwest (NE–SW) directions. The appearance of these configurations performs an essential role in the presence of the springs of the Gara and Siwa depressions oases.

### **The hydrogeological setting (water-bearing formation)**

In the GO and SO, the groundwater is exhibited in different water-bearing formations. These formations are (the Miocene fractured limestone shallow aquifer, the Eocene fractured limestone, and the deeper aquifer of Cretaceous Nubian sandstone).

The Miocene and Eocene water-bearing formations describe the tertiary carbonate aquifer system. It consists of carbonate (limestones and dolomite) rocks intercalations with sandstone, shale, siltstone, and evaporates sediments in certain sections, 450–600 m in thickness. The water supply system is under confining conditions (*El Hossary, 2013*). The aquifer of Nubian sandstone is overlaid by the tertiary carbonate aquifer (Eocene–Miocene). The low permeability shale and clay layer separate the fractured carbonate sections from the underlying Nubian sandstone. This layer is behaving as a cap rock and is between 60 m to the west and 250 m to the east in thickness (*El Hossary, 2013*). The major source of recharge for the aquifers is the upward leak from the NSSAS (*Ibrahim, 1991; Dahab, 2004*). The interesting one for our study is The Miocene carbonate aquifer (shallow aquifer). The Miocene fractured limestone involves the floor of the depression under the surface part. This aquifer achieves a thickness of about 250 m realized by medium-hard to hard limestone, white, sandy, and siliceous downward with intercalations of shale and marl. The field survey of the private shows that the shallow wells (less than 40 m depth) have low yield accomplish 240 m<sup>3</sup>/day (*El Hossary, 1999*). On the other hand, the wells with depths less than 150 m exhibit a zone of 80 m thick, consisting of hard limestone interbedded with shale has a yield of 960 m<sup>3</sup>/day (*El Hossary, 1999*). The productivity of this aquifer has varied from one place to another due to the variety of fracture occurrences and the extent of its relationship with the source of recharge (Nubian sandstone aquifer). The various drillings of RIGW (1996–1999) exhibit several zones of fractures inside the carbonate aquifers.

## 2.2. Geophysical methodology

Two geophysical techniques are used and integrated with this study to delineate the groundwater aquifer and examine its controlling parameters. The magnetic method is used to figure out the possible faulting systems that may control structurally the aquifers and the subsurface distribution of the magnetic susceptibilities related to different rock units, Moreover, the electrical survey is used to investigate the subsurface groundwater aquifer's electrical and hydraulic characteristics.

### Magnetic methods

The magnetic method of exploration is a simple, yet valuable and effective technique in different fields of shallow and deep exploration. It is implemented in many integrated studies aiming to delineate the structural setting (e.g. *Abdelazeem et al., 2021; Araffa et al., 2021; Azeem et al., 2014; Al-Garni et al., 2012*) and in groundwater studies (*Gobashy et al., 2021b; Al-Garni et al., 2006*) and exploration of the mineral (*Gobashy et al., 2022; Gobashy et al., 2020; Gobashy et al., 2021a; Abdelrahman et al., 2019*), groundwater contamination (*Rehman et al., 2019*).

The present study is based on the available aeromagnetic data from the survey conducted by *EGPC (1989)*. The survey was conducted by Egyptian General Petroleum Cooperation using airborne magnetic, the total magnetic intensity (TMI) measurements were carried out using the high-sensitivity (0.01 nT) airborne proton free-precision magnetometer (Varian, V-85). The magnetometer was mounted in a tail stinger. In addition, the Varian (VIW 2321 G4) single-cell caesium vapour was used as a base station magnetometer, (*Aero-Service, 1984*). The aeromagnetic data interpretation aims to delineate the regional structural setting of the Gara region and to examine the structural controlling parameters (folds and faults) of the shallow and deep groundwater aquifer of the depression. This survey data is re-digitized and processed to 674 data points and a reduced-to-pole map is calculated (Fig. 5). To evaluate the general structure of the Gara region, this map is subjected to several linear spatial filtering techniques. Also, two selected profiles (P1 & P2) perpendicular to each other are extracted (approximately 35 km and 55 km, respectively) and studied extensively.

The reduced to pole magnetic anomaly is calculated to minimize the dipolar nature of the geomagnetic field. A MATLAB<sup>®</sup> function is used to

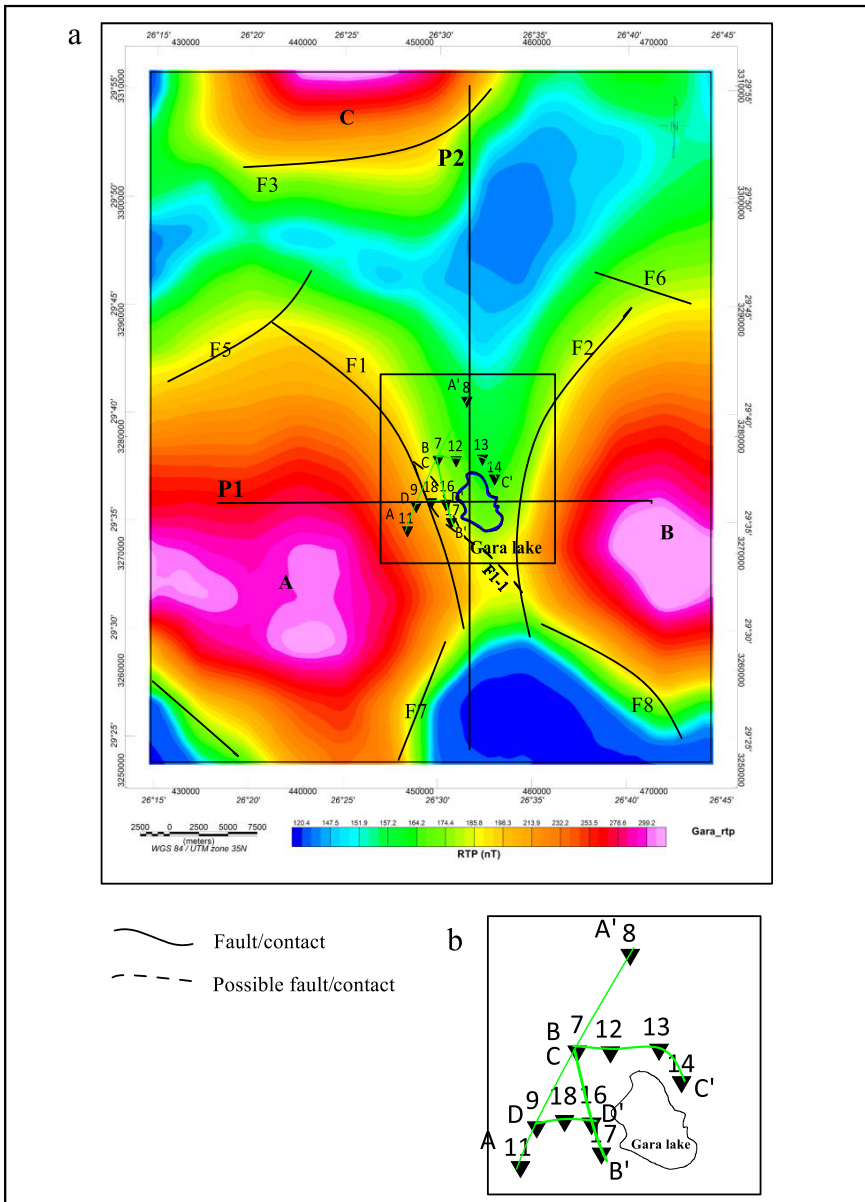


Fig. 5. (a) Reduced to pole magnetic anomaly map of Gara and (b) location of the measured electric VES's and geolectric sections.

deskew (normalize) the field based on the Fourier transform. The inclination and declination of the field are specified from the IGRF calculations as  $I = 42.17^\circ$  and  $D = 4.3^\circ$ , respectively. The filter transforms the regular grid of the total-field anomaly into new anomalies with new directions of magnetization and ambient field. The following steps are used: (1) the field was transformed using Fourier transform, (2) multiply by the phase filter and (3) inverse Fourier transform was used to transform to space domain as RTP field. Anomaly values were specified on the rectangular grid. The first-order derivatives are then calculated in all orthogonal Cartesian directions to enhance the spatial distribution of magnetic anomalies. Moreover, analytic signal (Nabighian, 1972) and tilt angle (Salem et al., 2008) are used to extract possible direction and depths to magnetic sources. The analytic signal is a complex function that makes use of Hilbert transform properties to detect geologic boundaries, faults, and dykes. It is effective for the interpretation of subsurface magnetic contacts (e.g., Nabighian, 1972, 1974). This method does not require prior knowledge of magnetization directions and thus does not require reduction-to-the-pole processing. A fault or geologic contact with susceptibility contrast can be extracted by tracking the maxima of the simple analytic signal, which is calculated from one vertical gradient and two horizontal (Nabighian, 1972, 1974, 1984; Roest et al., 1992). It is classically assumed that the causative sources are vertical or near-vertical, step-like geologic structures (Hsu et al., 1996; Nabighian, 1972; Roest et al., 1992) in this case the maxima are located directly over the boundaries of the structures. However, in the case of two maxima from two nearby parallel edges merging to one maximum and the half-width between the edges is less than the depth, an interpretation pitfall of using this method may arise (Atchuta Rao et al., 1981). For complete mathematics of the technique, the reader can be referred to Hsu et al. (1996). The tilt angle derivatives (Salem et al., 2008) on the other hand, is a simple and straightforward technique that assumes also vertical or near-vertical step structures and utilizes the second derivatives of the magnetic anomaly. In this technique, a linear equation is introduced to estimate the horizontal location and depth of magnetic sources without previous information about the nature of the sources. The source body information is obtained by finding structural indices (SI) using the estimated location parameters of the sources.

To quantitatively evaluate the subsurface magnetic anomalies across selected profiles P1 and P2, we carried out magnetic tomography analysis using regularized focused inversion. In this technique, the 2D half-space is subdivided into a large number of cells or blocks with unknown magnetic susceptibilities. The relative values of these susceptibilities are obtained through magnetic inversion. In brief, the solution of the inverse problem is transformed into the Tikhonov parametric functional's minimization  $P^\alpha$  (Portniaguine and Zhdanov, 1999):

$$P^\alpha(m) = \varphi(m) + \alpha s(m), \quad (1)$$

when,  $m_L < m < m_U$ , where,  $m$  is unknown parameter (magnetic susceptibilities of each cell) and  $\varphi(m)$  denotes a misfit functional error estimated as a model (norm) of the difference between the expected and observed (calculated) fields. The inequality restricting parameters are  $m_L$  and  $m_U$ , and  $s(m)$  is a function that helps to stabilize (stabilizer). These are based on the sample's magnetic susceptibility obtained in the research region that has been assessed.

### Geoelectrical methods

For decades, direct current (DC) surveys have been utilized to investigate groundwater resources worldwide. The geoelectric technique is generally associated with groundwater investigation and correlates the electrical properties of geological formations with their fluid content (Zohdy *et al.*, 1974; Ogilvy, 1970; Zohdy, 1965; Flathe, 1955 & 1970). Several investigations have been carried out in establishing aquifer geometry.

The geoelectrical cross-sections when correlated with the available geophysical, geological information, and the available wells, can provide information for the lithological, hydrogeological, and structural conditions within the studied area. Generally, the DC resistivity technique was proposed in this study for outlining the vertical and horizontal distributions of geologic formations, groundwater, and its quality. These objectives will be represented as depths and the thicknesses of the water-bearing structures. The obtained field data were corrected, analysed, and interpreted to obtain the specific parameters which define the layering models beneath the surface. Interpretation of (VESs) measurements was achieved by applying conventional (manual) and analytical procedures (Reynolds, 1997).

The initial model for analytical technology was presented with resistivity and thickness estimates from conventional interpretation. These methods involved using the (*IPI2WIN, 2000*) program to decrease RMS errors, which describe the performance comparison among the measurements on the field and the analytical curves since a low RMS value indicates more consideration (*Zohdy et al., 1974*). Four geoelectric cross-sections show the major structural components and geoelectric properties of the geological strata in the investigated region, models of the true final Resistivity generated from the assessed reversion of the resistivity data at every VES were used. Accordingly, vertical electrical sounding (VES) technique was conducted (VESs #7, #8, #9, #11, #12, #13, #14, #16, #17, and #18 as shown in Figs. 5 and 6) for exploring the resistivity variations at certain selected sites along profiles (A, B, C, and D) (Fig. 6) to define the variations of resistivity values with depth. The lateral variations were recorded throughout the constructed geoelectric cross-sections. The Schlumberger configuration, with AB/2 ranges between 1 and 400 m utilized in ten vertical electrical

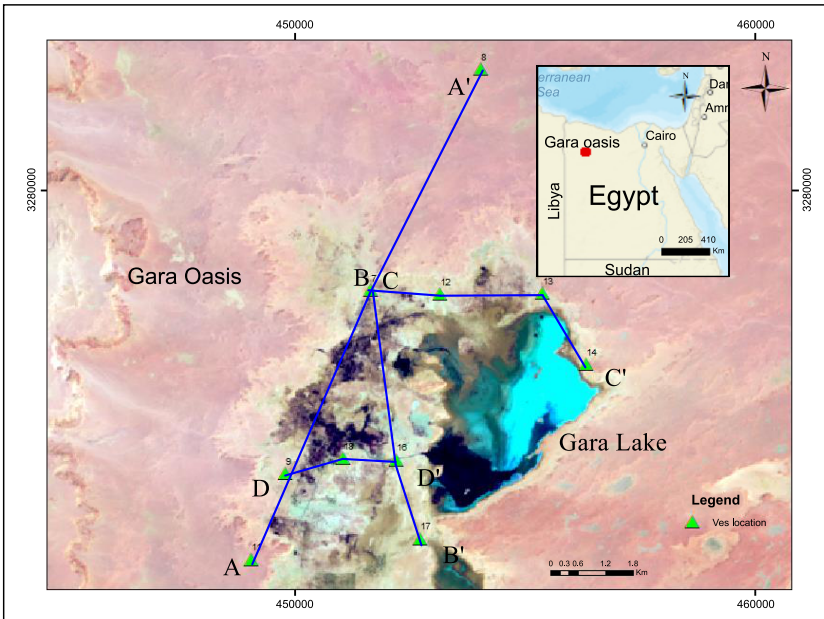


Fig. 6. Location of vertical electrical sounding (VES) as measured in Gara Oasis and the geoelectric cross-sections.

soundings (VESs). Intervals have been achieved in this area, so that the shallow Miocene carbonate aquifer depth may be achieved. The Syscal-Pro switch unit, made by IRIS Instruments in France, is used to estimate resistivity measurements.

Usually, an electrical resistivity survey is typically performed by introducing the current source into the ground through two electrode surface, which provides the best means of focusing in the earth, and two potential (voltage) electrodes, which measure the voltage differential to determine its subsurface resistivity distribution.

The present investigation utilizes a sample interval of one-sixth of a decade. According to *Zohdy (1989)*, however, because of the non-uniqueness inherent in the resistivity interpretation methods, any well-behaved model, in the sense that the layer resistivities do not oscillate, and whose computed curve fits the sounding curve within a few percent is an acceptable model. This means that the model error is a useful statistic for determining how well an inversion is performed.

Using the above technique of iterative interpretation in the present study, the interpretation of the acquired sounding data (employing the Schlumberger configuration) is carried out using a simple computer program. This program requires the digitized values of the apparent resistivity field curve and an initial model in the form of resistivity and thickness interval as input data. In addition to the values chosen for model parameters (resistivity and thickness), the mean error between estimated and observed data was acquired as output results for each step in the iteration process and may then be shown as contour maps.

The following steps have been used to interpret field data:

- a) Field curve matching to the conventional auxiliary technique curves (*Marsden, 1973; Mooney et al., 1966*);
- b) construction of a forward particular set model of a limited number of geoelectrical layers based on existing data collected from the boreholes in the investigation area as (the thicknesses and correspondence of resistivity) (*Patella, 1975*); and
- c) in the geoelectric modelling package, enter the initial geoelectric model of *Van Der Velpen (1988)*. The inversion of one-dimension (1D) modelling of each VES has been used in *Zohdy's* iterative method (*Zohdy, 1989*). The best match between the smoothed and calculated field curve

was performed using Iterations. The root mean square errors (RMS) are determined for the resultant models. Fig. 7a shows a field data example for VES (and the configuration of the array used), and Fig. 7b shows all 10 VESs used in this study.

The A-A', B-B', C-C', D-D' are the cross-sectional profiles, constructed from the ten measured VESs (#7, #8, #9, #11, #12, #13, #14, #16, #17, and #18) to elucidate the extension of Miocene aquifer (shallow aquifer) in GO (Fig. 6) and to illustrate the distribution over the researched area of the calculated resistivity parameters in the vertical plane (true resistivity and thickness). Results of magnetic interpretations are implemented in constructing the geoelectric sections. This includes the location of expected faults/or boundaries. The drilled deep wells in the area were also used to calibrate the geological information to be confirmed with the true resistiv-

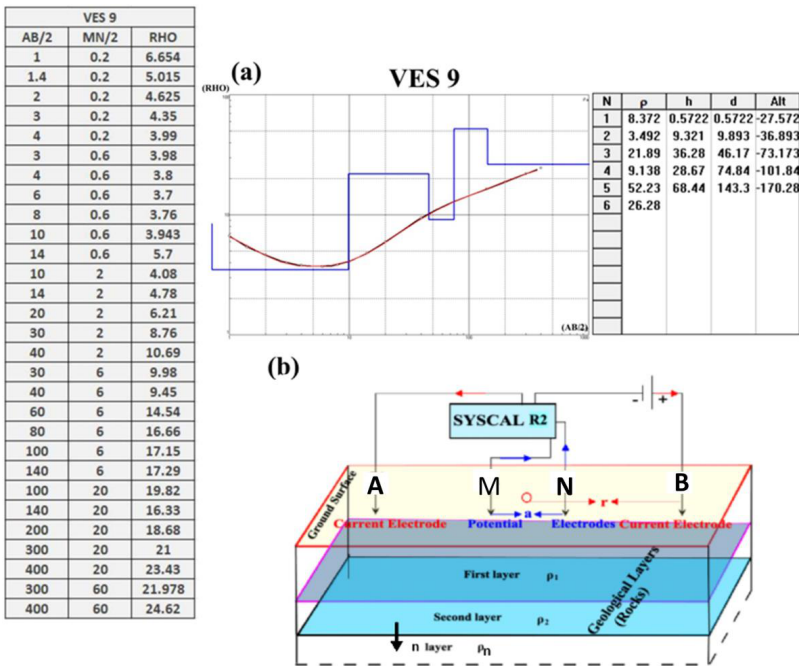


Fig. 7a. Example of field data for VES 9 with (a) the constructed one-dimensional inverse model with true resistivity, thickness, depth, and its topography to the top of each layer. (b) the Schlumberger configuration as used in this study. A and B are current electrodes, and M and N are potential electrodes.

ity values. Table 1 summarizes the layer characteristic properties (thickness and true resistivity) determined by quantitative interpretation. As a consequence, these characteristics are merged with previously collected geological information (*Flathe, 1976*) for the construction and development of the

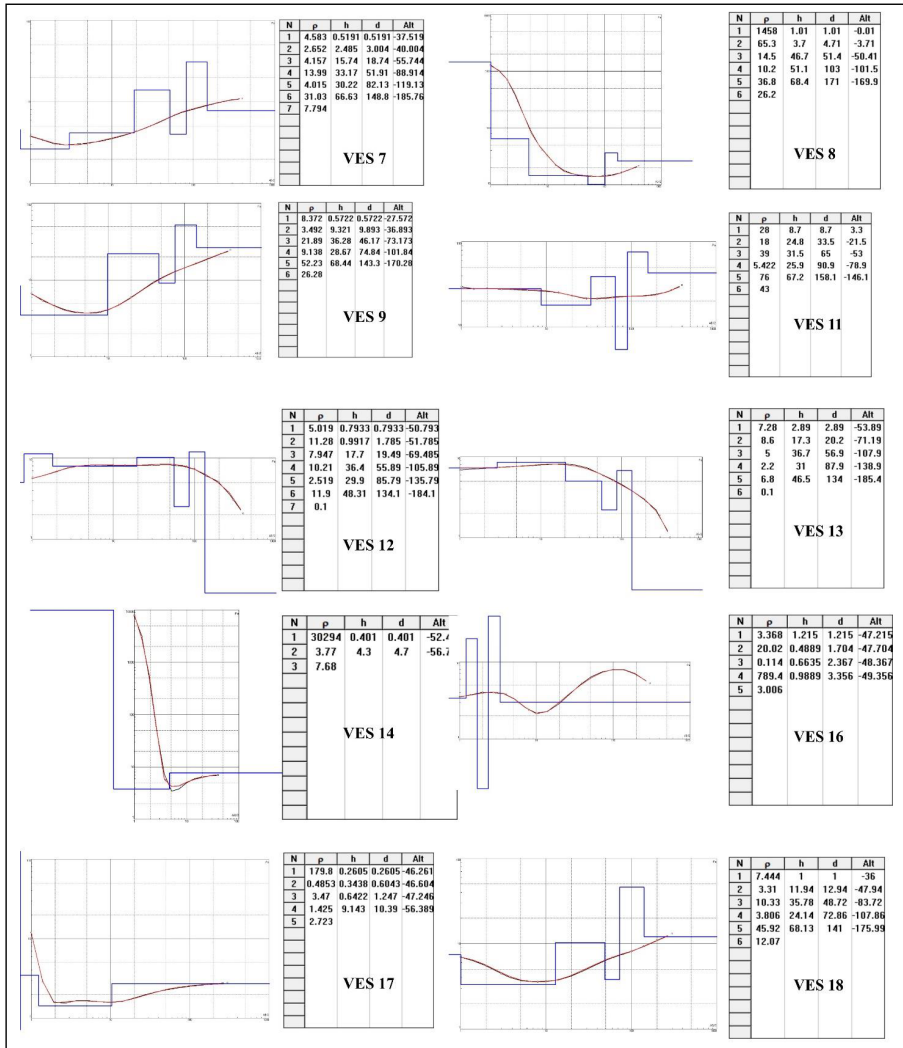


Fig. 7b. Data for the 10 VESs acquired in the GO and the one-dimensional inverse model for each VES with true resistivity, thickness, and depth to the top of each layer.

research region’s geological perspective and vision. In the cross-sectional profiles, each of the displayed vertical and horizontal scales is in meters, while the vertical scale indicates the depth relative to sea level, and the horizontal scale indicates the distance between the VESs along the section.

Table 1. Subsurface layers true resistivity and thickness.

VES No.	VES Name	S.L	$\rho_1$	h1	$\rho_2$	h2	$\rho_3$	h3	$\rho_4$	h4	$\rho_5$	h5	$\rho_6$	depth (m)
7	G 1	-37	7	3.08	4	16.23	14	33.8	4	30.22	31	65.49	7.6	185.2
8	G 2	1	1458	1.01	65	3.7	14	46.7	10	51.1	36	68.4	26	170
9	G 3	-27	13	5.7	7	9.5	22	40	9	27.7	51	60.9	24	170.8
11	G 5	12	28	8.7	18	24.8	39	31.5	5	25.9	76	67.2	43	146.1
12	G 6	-50	5.3	1.7	8	17.7	10	36.4	2.6	29.9	11.9	49.7	0.1	185.4
13	G 7	-51	6.8	2.2	8.6	17.3	5	36.7	2.2	31.1	6.8	47.2	0.1	185.5
14	G 8	-52	27390	0.4	3	4.6	1	18.6	0.9	31.1	1.9	47.2	0.1	154.9
16	G 10	-46	3.6	1	5.5	1.6	3	47.5	1.2	22.4	5.7	76.1	0.5	194.6
17	G 11	-46	188	0.4	1.9	2.5	1	47.5	0.9	22.4	4	76.1	0.2	194.9
18	G 12	-35	7.8	1.6	3	11.8	10	35.6	3.6	24	45.9	68.4	12	176.4

### Dar Zarouk Parameters

A geoelectric-sounding quantitative interpretation is relevant in the horizontal construction of stratified layers with a resistivity ( $\rho_i$ ) and a spatial thickness ( $h_i$ ) characteristic of each layer ( $i$ ) when specific accurate analyses of the data with electrical anisotropic ( $\lambda$ ) are available. And this consequently, Dar Zarouk (DZ) parameters could be used to explain and identify electrical anisotropy from the electrical vertical sounding VES, first proposed by *Maillet (1947)*.

Total transverse resistance (Tr), total longitudinal conductance (Sc), Average Longitudinal resistivity ( $\rho_L$ ), Anisotropic coefficient ( $\lambda$ ), and Transverse resistivity ( $\rho_t$ ) are the parameters. In geoelectrical soundings (VESs), various thickening ( $H$ ) and resistivity ( $\rho$ ) combinations play a vital role (*Zohdy et al., 1974*). They are used to distinguish between various groundwater characteristics and geological settings. Many authors have described the practical applications of these parameters (*Utom et al., 2012; Srinivas et al., 2012; Nwankwo et al., 2011; Ehirim and Nwankwo, 2010; Batayneh, 2009; de Oliveira Braga et al., 2006; Henriet, 1976; Singh, 2005; Singh et al., 2004; Mazáč et al., 1985; Zohdy, et al., 1974; Zohdy, 1965; Oteri,*

1981; Campbell, 1977; Worthington, 1975; Orellana, 1963; Flathe, 1955) They can be summarized as follows:

$$S_c = \sum_{i=1}^N \frac{h_i}{\rho_i}, \quad (2)$$

$$Tr = \sum_{i=1}^N h_i \rho_i, \quad (3)$$

$$\rho_L = \frac{H}{S_c}. \quad (4)$$

Also, the thickness and resistivity are employed to estimate the additional parameters anisotropy ( $\lambda$ ) and average transverse resistivity ( $\rho_t$ ).

$$\rho_t = \frac{Tr}{H}, \quad (5)$$

$$\lambda = \sqrt{\frac{\rho_t}{\rho_L}} = \frac{\sqrt{S_c Tr}}{H}, \quad (6)$$

where  $N$  defines the number of layers with resistivities  $\rho_1, \rho_2, \dots, \rho_n$  and thicknesses  $h_1, h_2, \dots, h_n$  for a unit square area and thickness of a block  $H = \sum_{i=1}^N h_i$ . The above parameters are calculated for a specific layer in the GO area to examine the aquifer characteristics.

An illustrative flowchart is given in Fig. 8 to summarize the successive steps followed in the application of different techniques for acquisition, processing, and interpretation.

### 2.3. Results and discussion

The study area's reduced-to-pole (RTP) magnetic anomaly map (Fig. 5) shows a 240 nT magnetic relief. Three major high magnetic anomalies can be distinguished, anomaly **A** to the west of Gara Lake, **B** to the east, and **C** to the north. These three anomalies are separated from the surrounded low magnetic background with possible magnetic contacts or faults. (F1–F8) as shown in Fig. 5a. The spatial analysis of the RTP map is carried out using derivative filters to examine the possible extent of the surface or subsurface magnetic contacts. The first derivatives of the three orthogonal directions are revealed in Figs. 9a,b & c. The peaks of these derivatives illustrate the possible magnetic susceptibility contrasts. This contrast may be of

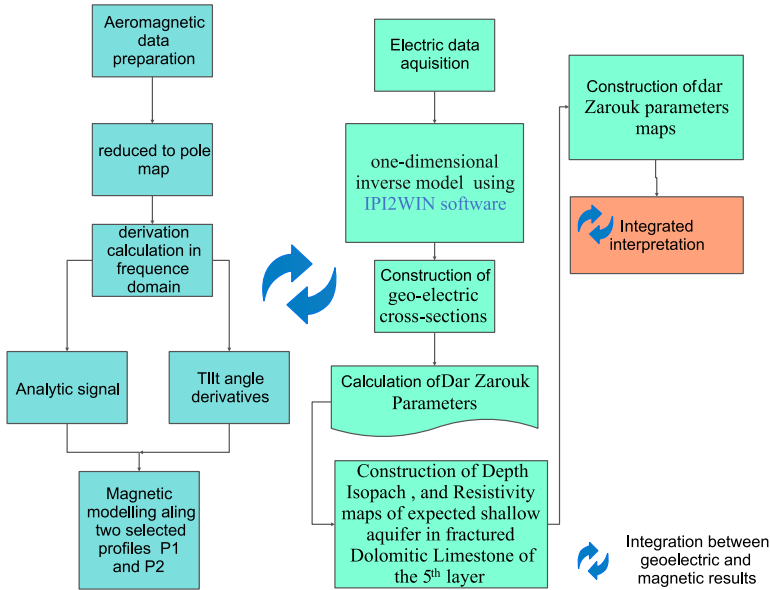


Fig. 8. An illustrative flowchart for the successive steps flowed in the application of different techniques for acquisition, processing, and interpretation.

deep origin (corresponding to the basement) or to any magnetized rock formations representing intra-sedimentary anomalously magnetic bodies. The total derivative and tilted maps (*Salem et al., 2008*) (Figs. 9d & e) peaks show possible NW–SE, EW, and NE–SW as common trends. These trends bound the major anomalies **A**, **B**, and **C** as shown in the RTP map (Fig. 5). The trend of NE–SW is a significant pre-Cambrian pattern with right-lateral movement. The rejuvenation is associated with a higher rate of northward movement in Arabia than in Africa (*Said, 1990*). The Erythrean faults fit with the NW–SE trend (*Said, 1962*) and the trend of the Suez Gulf (*Youssef, 1968*). During the Hercynian and Alpine orogenies, this trend was thought to be an old trend that was periodically renewed. The Tethyan trend, the E–W trend, is Egypt’s Precambrian basement’s oldest tectonic trend. The analytic signal on the other hand shows partially similar trends. Analysis of the tilt derivative map (Fig. 9e) shows possible basinal areas formed at the downthrown side of the proposed faults/contacts. Both the analytical signal map AS (Fig. 9f) and the tilt derivative map TD (Fig. 9e) were carried out to emphasize the short-wavelength magnetic anomalies which are

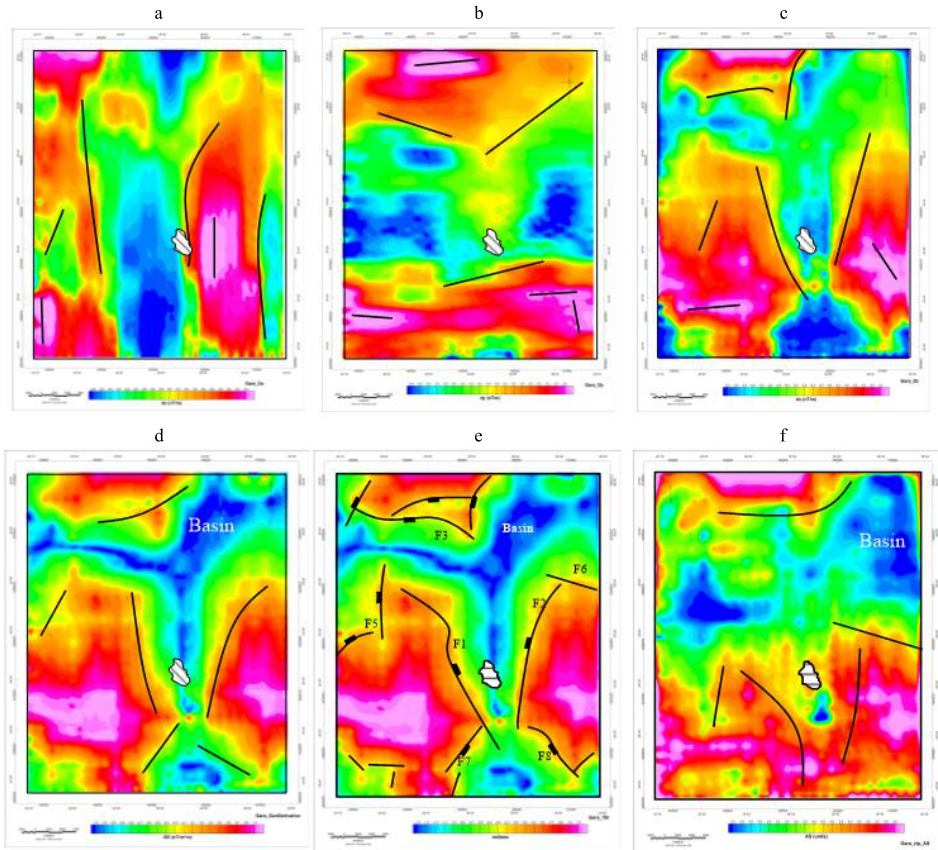


Fig. 9. The spatial filters were applied to the Gara area. The dx (a), dy (b), and dz (c) gradient filters, and variant filters generalized derivative (d), tilt derivative (e) and analytic signal (f).

mostly due to near-surface targets. Moreover, the AS map assisted to trace effectively magnetic anomaly trends and patterns along their strike. The detected basins constitute a large volume of non-magnetic sediments that form a suitable location for groundwater accumulations and flow.

Magnetic tomography shows regional variations in the subsurface magnetic susceptibilities that may be separated by a system of faults as shown in Figs. 10 and 11. Along profile P1, Fig. 10, the inversion shows a low magnetic anomaly is underlying the Gara lake, and bounded by western and eastern high magnetic anomaly zones. Two faults F1 and F2 control this

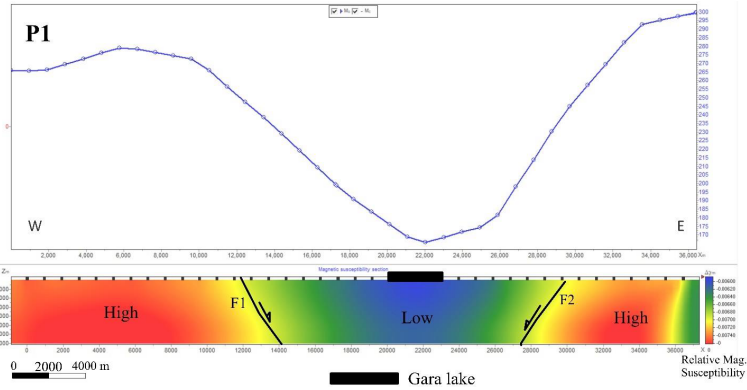


Fig. 10. Magnetic tomography across profile P1.

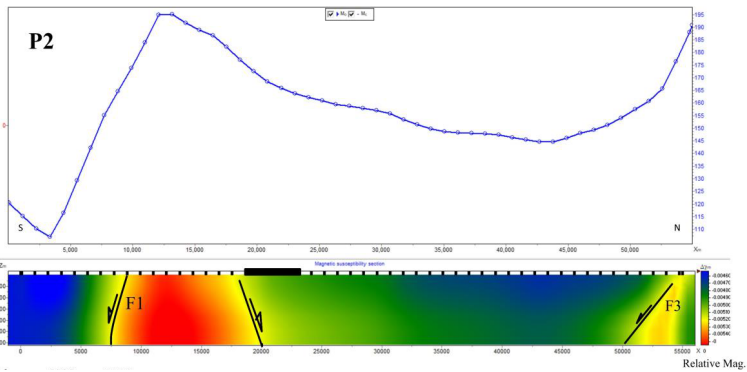


Fig. 11. Magnetic tomography across profile P2.

structural pattern. Similarly, inversion along profile P2 shows a southern high magnetic anomaly zone separated from the northern low susceptibility zone by a fault F1. Toward the north, the relative magnetic susceptibility decrease. These zones of high magnetic susceptibility may be related partially to the glauconitic sand with iron oxides concretions exposed at Naqb Al-Ahmer (southwest Gara lake, Fig. 3f) and may be extended with considerable concentrations at the subsurface. Particularly this high magnetic anomaly may reflect economic iron ore concentration in this zone.

The evaluation of the Geoelectric profiles across GO, on the other hand, reveals that Gara’s common calculated subsurface resistivity model consists

of six major resistivity layers. In general, they are represented by the four geoelectric cross-section profiles A–A', B–B', C–C', and D–D' (Figs. 12 to 15) and described spatially as follows:

1) The first layer (Figs. 12 to 15) depicts a Wadi Fill-deposit surface overburden layer with true resistivity values ranging from 3.6 to 27390  $\Omega$ .m, which correlates to alluvium deposits of limestone, sandstone, and clay. While the thickness of this layer ranges between 0.4 to 8.7 m. This layer is observed in the four profiles along the GO area. VESs (13, 14, 16, and 17) are close to the Gara lake and contain sabkha deposits (silt, sand, clay, and salt) due to lake evaporation. These are mixed with the surface deposits (slats, sandstone, clay, and limestone) and measured as highly conducting layers. Moreover, it will affect the induced electric energy pulsed within the subsurface and force the electric current to move horizontally within the highly conducted layer, consequently, the energy will travel vertically a few meters in the subsurface. In sections (A–A', B–B', Figs. 12 and 13) the discontinuity of the geoelectrical indicates a presence of a fault located between VESs (7, 16 and 7, 9).

2) The second layer represents a subsurface overburden layer of dry sandstone with some clay deposits (clayey sandstone). The true resistivity values range between 1.9 to 65  $\Omega$ .m, which is comparable to sandstone and clay. The layer's thickness ranges from 1.6 to 24.8 m and is constantly defined in the four profiles that develop all along GO area.

The highest resistivity value is 65  $\Omega$ .m, indicating less clay and more sandstone, while low resistivity values (1.9  $\Omega$ .m) indicate less sandstone and more clay since clay is more conductive than the dry sand so it has low resistivity. The red dashed lines in profiles (B–B', C–C' Figs. 13 and 14) corresponding VESs (14 and 17) represents a continuity of these layer from the previous VESs. This agrees with the drilled well within the area projected on the same profile.

3) The third layer represents a subsurface overburden layer of wet sandstone and fractures limestone deposits (calcareous sandstone) due to medium range values of resistivity within this layer with true resistivity values ranging between 1 to 39  $\Omega$ .m which is comparable to wet sandstone and fractured limestone (calcareous sandstone). The thickness varies from 18.6 to 47.5 m and it is continually observed in the four profiles.

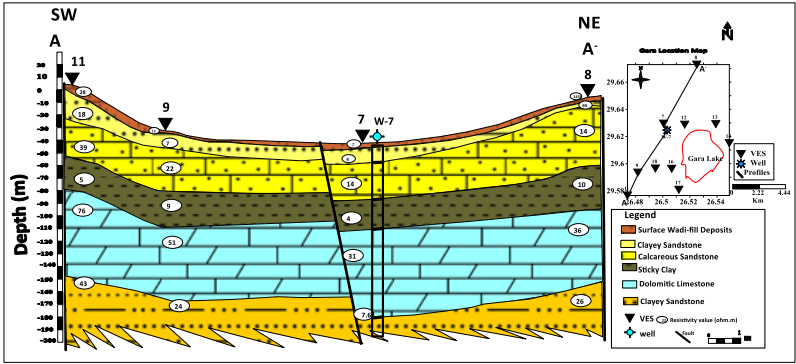


Fig. 12. Geoelectric cross-section A-A'.

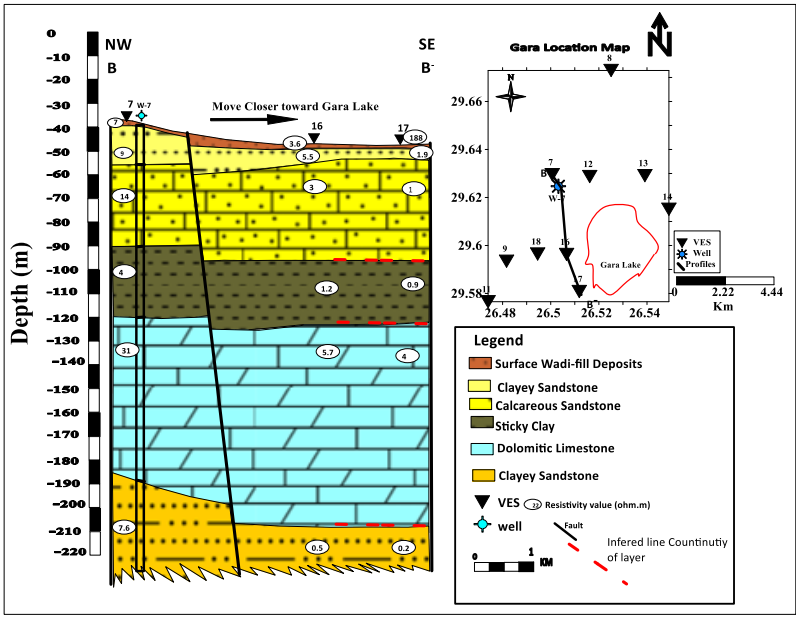


Fig. 13. Geoelectric cross-section B-B'.

The highest resistivity value (39 Ω.m) is observed below VES 11 that is away from the lake, so the amount of salinity and seepage is low and started to increase toward the Gara Lake. The lowest recorded resistivity values of this layer range from 1 to 10 Ω.m in all the other VESs (12, 13,

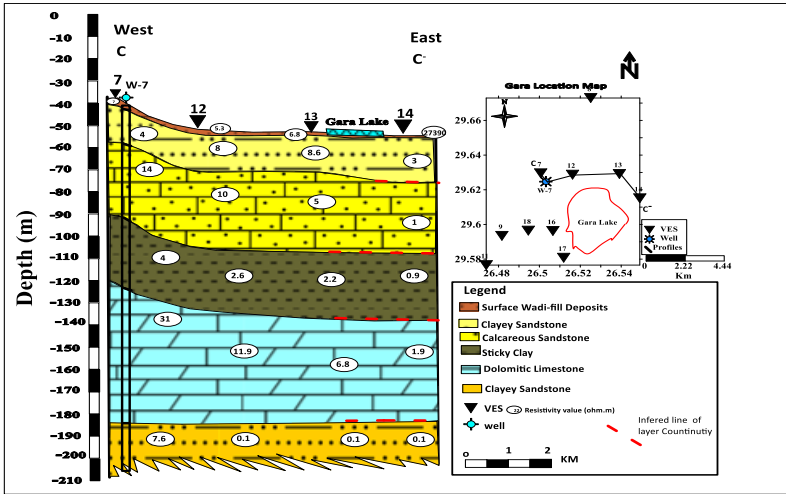


Fig. 14. Geoelectric cross-section C-C'.

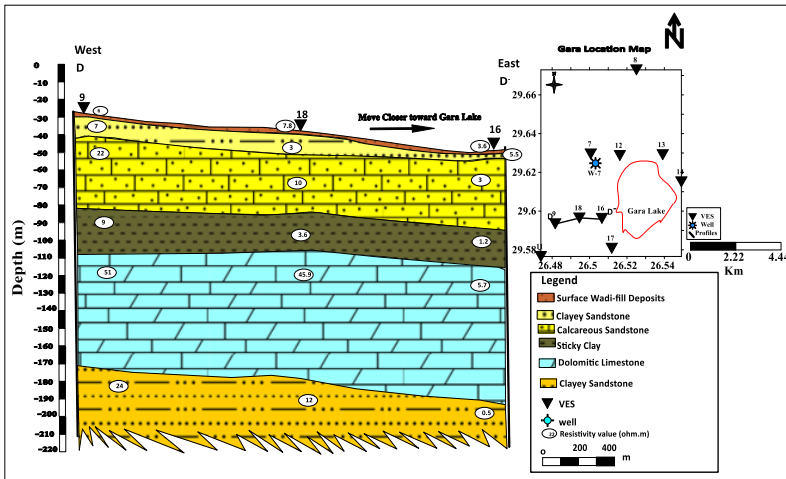


Fig. 15. Geoelectric cross-section D-D'.

- 14, 16, 17, and 18) representing a high concentration of sandstone and fractured limestone (calcareous sandstone).
- 4) The fourth layer represents a subsurface overburden layer of sticky clay with true resistivity values ranging between 0.9 to 10  $\Omega.m$  indicating

a highly clay content. The thickness varies from 22.4 to 51.1 m. The maximum resistivities vary from 4 to 10  $\Omega$ .m. are recorded at VESs 7, 8, 9, 11, 12, and 18. Those are away from the lake, so the amount of salinity and seepage is less and started to increase when moving in all directed toward the Gara Lake. The low resistivity values ranged between 0.9 and 4  $\Omega$ .m under all the other VESs (13, 14, 16, and 17) represented highly amount of saturation of the seepage of the lake. The red dashed lines in profiles (B–B', C–C', Figs. 13 and 14) below VESs (14 and 17) show the continuity of these layers from the previous VESs. This is confirmed from the well data. They are not observed clearly due to the masking of the energy dissipated horizontally within the highly conducted layer.

- 5) The fifth layer represents a subsurface overburden layer of fractured dolomitic limestone with true resistivity values varying between 1.9 and 76  $\Omega$ .m. This corresponds to dolomitic limestone that is cemented with some clay. The thickness varies from 47.2 to 68.4 m as observed in all profiles. The resistivity values vary from 11.9 to 76  $\Omega$ .m as measured in VESs 7, 8, 9, 11, 12, and 18. In the later VES, VES 18, which is away from the lake, the amount of clay that is cemented within it and seepage are less around them and started to increase toward the Gara Lake. The low resistivity values ranged from 1.9–11.9  $\Omega$ .m under all VESs (13, 14, 16, and 17) represented the presence of cemented clay and the high amount of saturation of seepage from the lake with the fractures. The red dashed lines found in profile (B–B', C–C', Figs. 13 and 14) and below VESs (14 and 17) represents a continuity of these layer from the previous VESs and also confirmed with the well within the area on the same profile.
- 6) The sixth and last layer represents a subsurface overburden layer of sandstone intercalated with some clay (clayey sandstone) with true resistivity values ranging between 0.1 and 43  $\Omega$ .m which is sandstone intercalated with some clay (clayey sandstone). The top of this layer is continuously observed in the four profiles along the GO area.

The high resistivity values vary from 12 to 43  $\Omega$ .m. These are shown in VESs 7, 8, 9, 11, 12, and 18, hence, the amount of clay that is intercalated within it and the seepage of the lake is less around them and started to increase when moving in all directions toward the Gara Lake. The low

values of resistivity ranged from 0.1 to 12  $\Omega$ .m under VESs (13, 14, 16, and 17) denoted the presence of intercalated clay and high amount of saturation of seepage brackish water from the lake within the porous.

After correlating these sections with the Upper Zone of Gara (drilled deep well (W-7)) and field observations in the studied area, the geoelectrical profiles confirm that:

- 1) The 1st layer represents a surface overburden layer of Wadi fill-deposits (alluvium deposits of limestone, sandstone, and clay).
- 2) The 2nd layer is correlated and composed of sandstone with clay (clayey sandstone).
- 3) The 3rd layer is correlated and composed of wet sandstone and fracture limestone (calcareous sandstone), this fractured and porous sandstone is filled with brackish water.
- 4) The 4th layer is correlated and composed of sticky clay that is affected with brackish water due to seepage on VESs that surrounded the lake.
- 5) The 5th layer is correlated and composed of fractured dolomitic limestone that is cemented with some clay that is affected with brackish water due to seepage on VESs that surrounded the lake. It's important to mention that, the brackish to slightly saltwater that filled the fractures of carbonate Miocene rocks (limestone or dolomite) affects the resistivity values and causes the reduction of these resistivities. The condition of this layer represents a possible shallow aquifer in the region.
- 6) The 6th layer is associated and comprised of sandstone intercalated with some clay (clayey sandstone) that is affected with brackish water due to seepage.

### **Shallow aquifer fractured dolomitic limestone of the 5th layer**

To examine the conditions of the 5th layer fractured dolomitic limestone, depth and resistivity maps were constructed.

The iso-contour depth map of the possible shallow aquifer in the fractured dolomitic limestone layer (Fig. 16a & Table 2) gives the depth to the wet layer across the area. The depth varies between 54 and 102 m (Fig. 16a). It shows an increase of depth toward (northern, central, and SW). While depth decreased toward the (eastern and SW) part. On the other hand, the

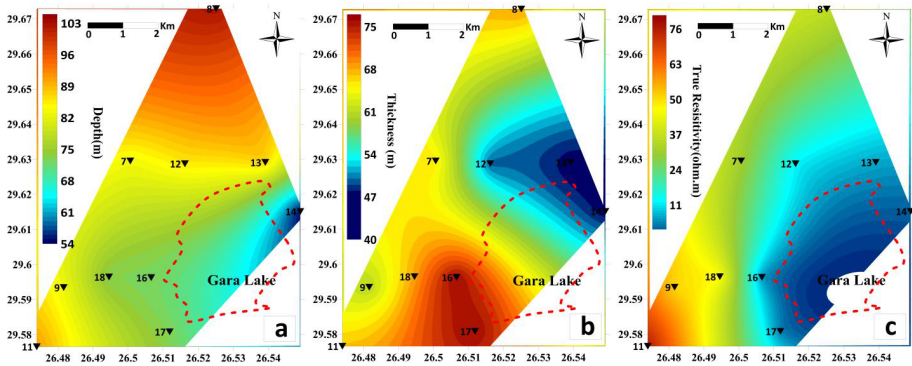


Fig. 16. Depth (a), isopach (b), and resistivity (c) maps of expected shallow aquifer in fractured dolomitic limestone of the 5th layer.

Table 2. Depth, thickness, and true resistivity of the possible shallow aquifer in the fractured dolomitic limestone layer.

VES No.	depth to 2nd aquifer 5th layer (m)	thickness (m)	true resistivity ( $\Omega$ .m)
7	83.33	65.49	31
8	102.51	68.4	36
9	82.9	60.9	51
11	90.9	67.2	76
12	85.7	49.7	11.9
13	87.3	47.2	6.8
14	54.7	47.2	1.9
16	72.5	76.1	5.7
17	72.8	76.1	4

isopach map of the aquifer gives a thickness of the wet layer across the area. The thickness varies between 40 and 73 m (Fig. 16b). It shows increasing in thickness toward (northern, western, southern, and SW) parts and reaches a maximum thickness that occurred at VESs (16 & 17) at the Southern part. While thickness decreased toward (eastern, and NE) parts and reach to minimum thickness occurred toward VESs (12, 13, and 14).

The iso-true resistivity map, on the other hand, was generated at an interval of (6  $\Omega$ .m) and is shown in Fig. 16c. It shows the resistivity distribution across the study area which varies from a very small value (0.5  $\Omega$ .m) to (70  $\Omega$ .m) since this very small value (0.5  $\Omega$ .m) due to the invasion of lake salinity with the high effect of brackish to saline water. The resistivity is

highly increased at each of (northern, and SW) parts of the area at VESs (7, 8, 9, 11, and 18) while it attains a maximum at VES 11 as it's away from the lake effect. On the other hand, it decreases at VESs (12, 13, 14, 16, and 17) toward eastern–SE parts. The resistivity values on this map indicate the wet fractured dolomitic limestone layer if filled with brackish to saline water.

### **Estimation and interpretation of Dar Zarouk parameters (DZ) for dolomitic limestone aquifer of 5th layer**

The DZ parameters are calculated for GO for the dolomitic limestone aquifer of the 5th layer. The following represents the results of this analysis:

- a) As indicated in Table 3 and Fig. 17a, total longitudinal unit conductance ( $S_c$ ), was calculated by integrating resistivity data from 10 (VESs) with an interval of 0.5 Siemens units to generate an  $S_c$  contour map. The high  $S_c$  values indicate low aquifer transmissivity with  $S_c$  values, varying from 0.003 to 8 S. The  $S_c$  variation from one place to another has been utilized to describe changes in the overall thickness of low resistivity materials in a qualitative sense (*Henriet, 1976; Zohdy, 1989*). An increase in the value of longitudinal conductance may correspond to an increase in clay content and thus, a reduction in transmissivity. The clay overburden which gives relatively high longitudinal conductance protects the underlying aquifer. The lowest values of  $S_c$  could be noticed in Fig. 17a at the northern, southern, and western parts. In addition to the middle part of the eastern side while highly increased at the central part, based on *Oteri (1981)* longitudinal conductance decreased may suggest decreased infiltration of seawater or decrease in water salinity (low clay content). The increase of the longitudinal conductance behaviour might thus be regarded as a reduction of the transmissivity.
- b) Total transverse resistance ( $Tr$ ) is used to investigate variations in the thickness of high resistivity material as well as their transverse resistance (*Zohdy, 1989*). Increasing  $Tr$  values are indicative of an increase in the thickness of the high resistivity materials. as shown in Table 3 and Fig. 17b, a contour map of  $Tr$  values of the study area was produced by using the resistivity data of 10 (VESs) sounding stations with a contour interval of 200000  $\Omega.m^2$  unit. Homogeneity in the total transverse resistance could be explained throughout the study area, except at the

eastern and south-eastern parts where an anomalous increase in the (Tr) could be observed. Based on *Niwas and Singhal (1981)*, there is a direct relationship between transmissivity and transverse resistance. They stated that the chemical quality of the groundwater within the evaluated zone remains relatively uniform. As a result, the present Tr map reveals a homogeneous distribution of electrical transmissivity across the study region, except the above-mentioned sections with high Tr values. The greatest transverse resistance value most likely represents the highest auriferous zone transmissivity values (*Kumar et al., 2001; de Oliveira Braga et al., 2006*). So the eastern and south-eastern parts of the area have good transmissivity because of the high value of Tr values as shown in the map.

- c) The longitudinal resistivity ( $\rho_L$ ) and the average transverse resistivity ( $\rho_t$ ) are constructed by combining the longitudinal and transverse resistivity values of the 10 (VESs) geoelectrical soundings collected in the research region (Figs. 17c & 17d). The contour interval of this map is 2000  $\Omega.m$  as shown in Figs. 6c & 16d both of ( $\rho_L$ ) and ( $\rho_t$ ) are the same distribution that indicates a homogeneous distribution.
- d) Anisotropy ( $\lambda$ ) as demonstrated in Table 3 has root mean square resistivity and is dimensionless. It reflects the electrical anisotropy's areal distribution over the research region. For altering electric resistivity in both horizontal and vertical directions, electric anisotropy was determined. In most geologic settings, the anisotropy coefficient is 1 and does not exceed 2 (*Zohdy et al., 1974*). The anisotropic factor is increased by a compact and complicated rock at shallow depth (*Keller and Frischknecht, 1966*). The 1.0 anisotropy regions with 10 VESs in Table 3 are categorized as high groundwater prospects (high porosity and permeability) (*Jagadeeswara Rao et al., 2003*). The variation of the isotropic layers (where anisotropic = 1.0) might become a heterogeneous and anisotropic equivalent structure has been well established. As shown in Table 3 the values of anisotropy  $\lambda = 1$ , which mean it is homogenous.

**Contour maps of Dar-Zarouk parameters for dolomitic limestone aquifer of 5th layer that's is more interested**

The 2D analysis of DZ parameters to examine the spatial distributions of the aquifer parameters is demonstrated as follows:

Table 3. Values of Dar-Zarrouk (DZ) parameters. The total transverse unit resistance (Tr), total longitudinal unit conductance (Sc), and longitudinal resistivity ( $\rho_L$ ) at all 10 (VESs) in a fully examined region with depth ( $H$ ) to the aquifer, average transverse resistivity ( $\rho_t$ ), and anisotropy ( $\lambda$ ).

Parameters of expected shallow aquifer fractured dolomitic limestone of the 5th layer									
VES No.	$H$ (m)	Sc (siemens)	Tr ( $\Omega.m^2$ )	$\rho_L$ ( $\Omega.m$ )	$\rho_t$ ( $\Omega.m$ )	$\lambda$	layer resistivity ( $\Omega.m$ )	electric conductivity EC (dS/m)	TDS (mg/l)
7	148.82	2.480	8929.2	60	60	1	31	0.322	206.451
8	170.91	0.107	270550.53	1583	1583	1	36	0.277	177.777
9	143.8	1.409	14667.6	102	102	1	51	0.196	125.490
11	158.1	0.952	26244.6	166	166	1	76	0.131	84.210
12	135.4	3.582	5118.12	37.8	37.8	1	11.9	0.840	537.815
13	134.5	4.574	3954.3	29.4	29.4	1	6.8	1.470	941.176
14	101.9	0.003	2791733.92	27396.8	27396.8	1	1.9	5.263	3368.421
16	148.6	7.821	2823.4	19	19	1	5.7	1.754	1122.807
17	148.9	0.760	29154.62	195.8	195.8	1	4	2.5	1600
18	141.4	2.0111	9940.42	70.3	70.3	1	45.9	0.217	139.433

### Contour maps of apparent resistivities at constant AB/2

The present study’s field measurement results are provided as a qualitative interpretation (maps of iso-apparent resistivity). Five apparent resistivity contour maps are constructed at  $AB/2 = 10, 100, 200, 300,$  and  $400$  m. Each spacing option is determined by the variation among them. The variations in electrical resistivity on the horizontal scale are depicted by these maps, at depths of 4, 40, 80, 120, and 160 meters, respectively (*Roy and Elliot, 1981*).

- a) At  $AB/2 = 10$  m, the map of iso-apparent resistivity is exhibited (Fig. 18a). At a depth of about 4 meters, this map illustrates the interchange of lateral variation across a horizontal plane perspective. It illustrates relatively high apparent resistivity values ranging from (11 – 18  $\Omega.m$ ) at VESs (20 and 44) indicating that its wadi fill-deposits with less sabkha content and away slightly from the effect of lake salinity. While it has low apparent resistivity values ranging from (1 to 20  $\Omega.m$ ), at VESs (7, 11, 12, 13, 14, 16, 17, and 18) indicate that the sabkha and lake salinity are the most dominant and controlling constituent of the wadi fill deposits.

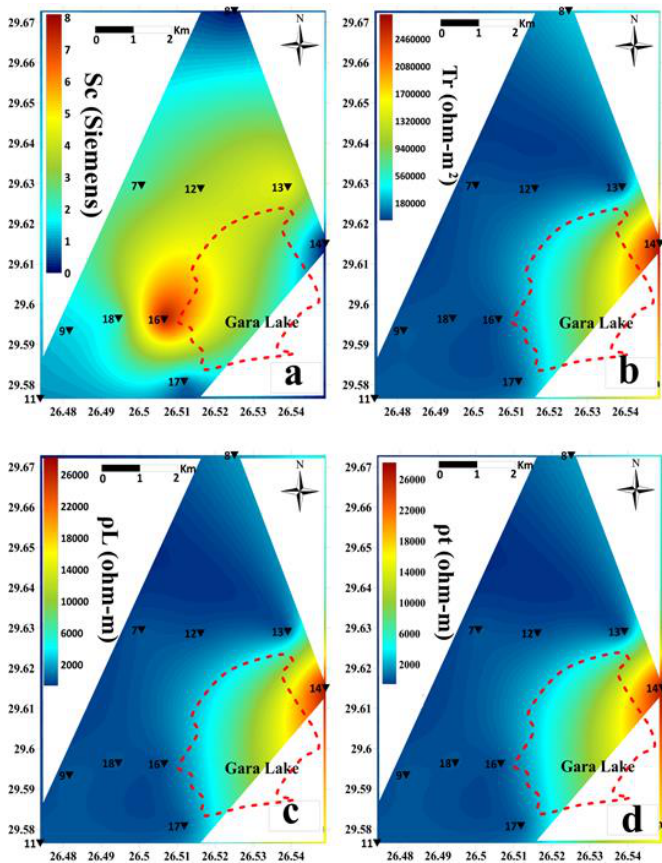


Fig. 17. Contour maps of the  $S_c$  (a),  $T_r$  (b),  $\rho_L$  (c), and  $\rho_t$  (d). Location of geoelectrical soundings are shown as inverted black triangle.

b) At  $AB/2 = 100$  m, the map of iso-apparent resistivity is exhibited (Fig. 18b). At a depth of about 40 meters, this map illustrates the interchange of lateral variation across a horizontal plane perspective. It shows relatively high apparent resistivity values ranging from (10–18  $\Omega.m$ ) at the surrounding VESs (7, 8, 9, 11, and 18) in northern, western, NW, NE, and SW parts indicate that a high amount of filling sediments that's indicated porous medium (clayey sandstone) based on the geological explanation from the geologic well, with slightly brackish water effect from the lake or less salinity effect. In another way, there is an increase in

apparent resistivity towards the sediments, indicating that the invasion of lake water in these areas is decreasing at (northern, western, NW, NE, and SW) parts.

The electric resistivity values ranged from (2–8  $\Omega$ .m) at VESs (12, 13, 14, 16, and 17) decrease from central to the eastern, southern, and SE parts towards the Gara lake indicate that the most more effect of lake salinity.

- c) At  $AB/2 = 200$ , and 300 m, the map of iso-apparent resistivity is exhibited (Figs. 18c, and d). These two maps explain the lateral variation exchange over a horizontal plane view at a depth of around 80 to 120 meters they are near to similarity due to approximately the invasion within the same layer (dolomitic fracture limestone) based on the geological explanation from the geologic well. they explain relatively high apparent resistivity values ranging from (11–25  $\Omega$ .m) at the surrounding VESs (7, 8, 9, 11, and 18) in northern, western, NW, NE, and SW parts indicate that a high amount of filling sediments of dolomitic fracture limestone that's indicated porous medium with slightly brackish water effect. That means apparent resistivity increases towards the sediments at (northern, western, NW, NE, and SW) parts.

The electric resistivity values ranged from (1–9  $\Omega$ .m) at VESs (12, 13, 14, 16, and 17) that decrease from central to the eastern, southern, and SE parts towards the Gara lake indicate that the most more effect of lake salinity and filled with brackish to slightly saltwater.

- d) At  $AB/2 = 400$  m, the map of iso-apparent resistivity is exhibited (Fig. 18e). At a depth of about 160 meters, this map illustrates the interchange of lateral variation across a horizontal plane perspective. It represents (clayey sandstone) based on the geological explanation from the geologic well. They explain relatively high apparent resistivity values ranging from 11 to 25  $\Omega$ .m at the surrounding VESs (7, 8, 9, 11, and 18) in Northern, Western, NW, NE, and SW parts indicate that a high amount of filling sediments of dolomitic fracture limestone that's indicated porous medium with slightly brackish water effect. That means apparent resistivity increases towards the sediments at northern, western, NW, NE, and SW parts.

The electric resistivity values ranged from 1 to 9  $\Omega$ .m at VESs (12, 13, 14, 16, and 17) that decrease from central to the eastern, southern,

and SE parts towards the Gara lake indicate that the most more effect of lake salinity and filled with brackish to slightly saltwater.

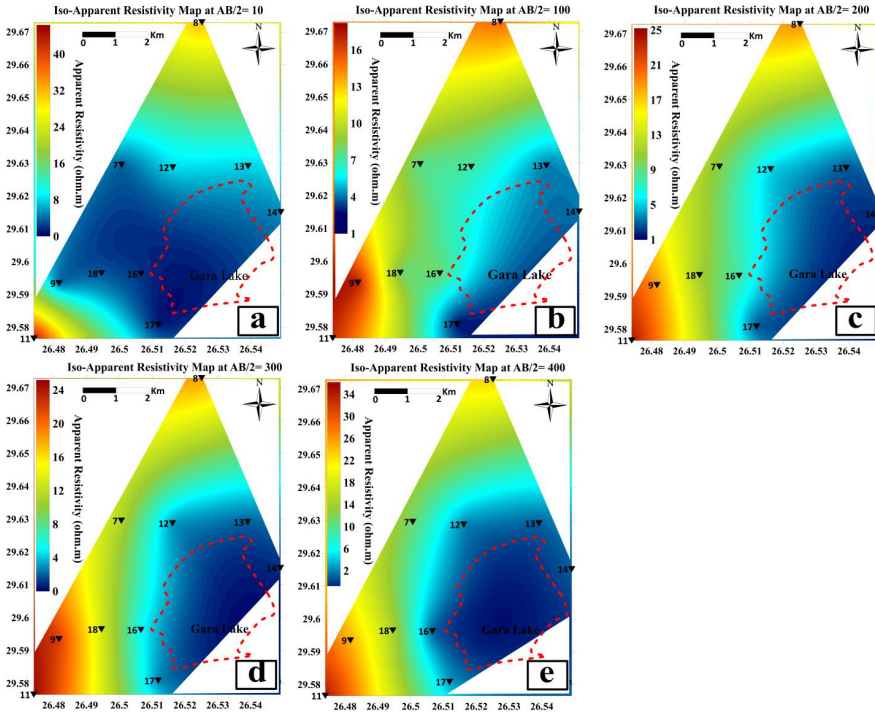


Fig. 18. Contour maps of apparent resistivities at constant AB/2 = 10 (a), 100 (b), 200 (c), 300 (d) and 400 m (e).

**The relation between true resistivity and groundwater salinity (TDS)**

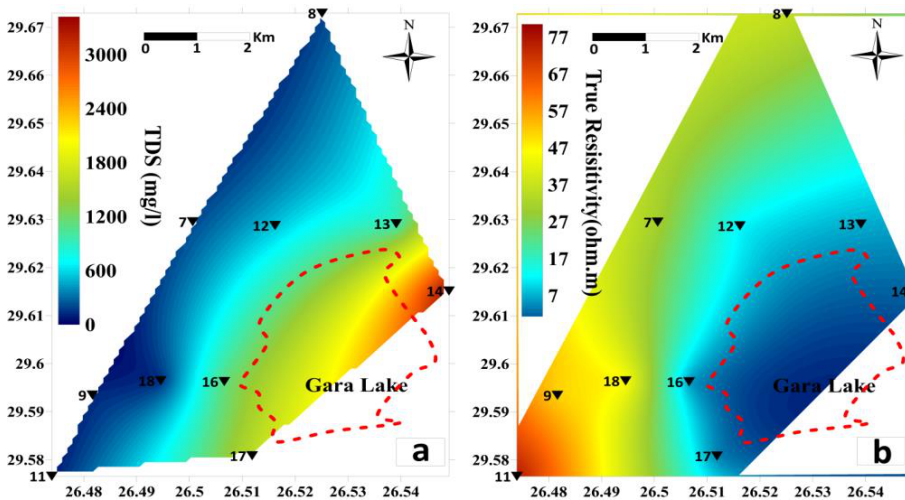
The salinity of groundwater total dissolved solids (TDS) at various depths can be predicted utilizing relationships based on measured VESs, much quicker than analysis of water samples and traditional digging methods (Attwa et al., 2016). According to Iyasele et al. (2015), as well as Hem (1970), the combination of total dissolved solids (TDS) and electric conductivity (EC) is as follows:

$$\text{Total dissolved solids (TDS)}_{(\text{ppm})} = 640 * \text{EC (dS/m)}, \tag{7}$$

where  $\rho_w = 1/\text{EC}$ . The electric groundwater resistivity ( $\Omega.m$ ) is denoted by

$\rho_w$ , while the electric groundwater conductivity (dS/m) is denoted by EC (siemens/m = 10 \* deci-siemens/m).

Figure 19a and Table 4 show the salinity (TDS of aquifer water) in the research region. The results were computed from the calculated VES resistivities. It is found that the maximum groundwater salinity (TDS) is less than 600 ppm in all VESs except VESs (13, 14, 16, and 17) where the TDS values exceed 600 ppm due to being close to the Gara lake. On the other hand, the lowest measured value of TDS was (less than 100 ppm) at VES 11 toward the South Western part of the research region. The maximum recorded value is (3368 ppm) at VES 14 toward the eastern part. Based on the salinity values determined by the aquifer and evaluated salinity hazard through TDS and EC (Iyasele et al., 2015; Carrow and Duncan, 1998) as given in Table 4 the aquifer can be described as fresh, marginal, and slightly brackish to saline water.



v Fig. 19. Salinity (TDS) (a), and true resistivity (b), maps of the study area, estimated via the results of geoelectrical sounding (VES).

Figure 20a exhibits the salinity (TDS) of water samples covered by field analysis and its distributions; it shows the TDS increase toward the eastern and south-eastern parts. While Figure 20b shows TDS estimated from the geoelectrical sounding measurement (VES), it reveals the same purpose of increment TDS toward the eastern, southern, and south-eastern parts.

Table 4. TDS and EC-based guidelines for assessing overall salinity hazards in variable quality irrigation water (Iyasele et al., 2015; Carrow et al., 1998).

salinity hazard class	EC (dS/m)	TDS (ppm)	description and use	management requirements
low (fresh)	< 0.75	< 500	drinking and all irrigation	no detrimental effects are expected
medium (marginal)	0.75–1.5	500–1000	most irrigation, adverse effects on ecosystems become apparent	moderate leaching to prevent salt accumulation
high (brackish)	1.5–3.0	1000–2000	irrigation of certain crops only; useful for most stock	turf species/cultivar selection, good irrigation, leaching, drainage
very high (saline)	> 3.00	> 2000	useful for most livestock	most salt-tolerant cultivars, excellent drainage, frequent leaching, intensive management

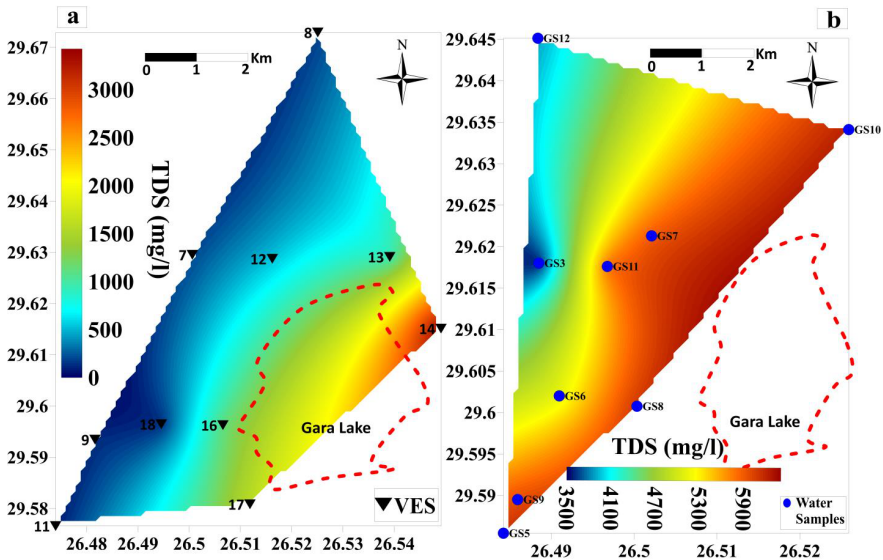


Fig. 20. The maps of salinity (TDS) of water samples measured in field (a) and TDS that were calculated from the geoelectrical sounding measurement (VES), (b).

### 3. Conclusion

Integrated interpretation of aeromagnetics and electric measurements could result in a valuable tool for the assessment of groundwater aquifers in hyper-arid and arid environments. In Gara Oasis, the shallow (Miocene carbonate), as well as the deep (Nubians sandstone) aquifers, are structurally controlled by a complex fault/magnetic contact system, evident from various filters that have been applied to the aeromagnetic data and the available drilling information. These contact trends northwest–southeast (NW–SE), east–west (E–W), and northeast–southwest (NE–SW) as common trends generated from the total derivative and tilt maps. The consequence of these trends is that subsurface water flow is directly controlled in all directions. The near-surface structurally controlled shallow Miocene carbonate groundwater aquifer described in the study region by dolomitic limestone (5th layer) is saturated by fresh to slightly brackish water. Six lithological layers that were successfully delineated by VESs conducted by the GO may be categorized into overloaded surface layers. The depth of the Miocene aquifer was shallow and ranged from 80 to 130 meters from sea level. Based on the combined aeromagnetic and geoelectrical investigations, the water quality derived from geophysical investigations and wells range from fresh to slightly brackish. Slightly brackish groundwater dominates the region, according to geoelectric cross-sections and resistivity values, while freshwater is found in isolated patches. The results demonstrate that the upper northern central portion of the GO, the southern central portion, and the western side of the GO have the most distinct aquifer possibilities that will demand future improvement strategies. The study may be applied to other depressions of similar conditions to extract the controlling parameters and sustainability of the different groundwater aquifers.

**Acknowledgements.** The fieldwork and VESs were collected through a Cairo University-funded initiative, Project ID #17-269 (PI: Prof. M. Gobashy). We would like to thank our colleagues from Cairo University’s Geophysics Department, Faculty of Science, for their help with the fieldwork, as well as their insight and knowledge, which significantly benefited the investigation.

**Funding.** This work’s fieldwork is supported by a project funded by Cairo University, Project ID #17-269.

**Conflicts of interest/Competing interests.** There are no conflicts of interest that are relevant to the content of this paper that the authors wish to declare.

**Data and materials are readily available.** Data sets created or analysed in the development of the current study are available from the corresponding author upon reasonable request.

**Code availability.** There is no code available in this work.

**Authors' contributions.** Gobashy M. M.: supplied the study's conception and design, acquisition of geophysical data, analysis and interpretation of magnetic data, authoring the paper, critically revising it for the importance of intellectual content, and final approval of the version to be submitted; Nazih M.: carried out the electric measurements acquisition (together with CU geophysics team), processing and interpretation with the help and supervision of the third author Arafa S., and drafting the manuscript. The interpretation is part of Mr. Nazih M.Sc. thesis; Soliman K. S.: supplied the acquisition of VES data together with Nazih M.; Abdelhalim A.: was responsible for the Geologic section, and geologic fieldwork.

## References

- Abdallah A., 2007: Assessment of salt weathering in Siwa Oasis (The Western Desert of Egypt). *Bull. Soc. Géogr. Égypte*, **80**, 65–83.
- Abdelazeem M., Fathy M. S., Gobashy M., 2021: Magnetometric Identification of Sub-basins for Hydrocarbon Potentialities in Qattara Ridge, North Western Desert, Egypt. *Pure Appl. Geophys.*, **178**, 3, 995–1020, doi: 10.1007/s00024-021-02678-2.
- Abdelazeem M., Salem Z. E., Fathy M. S., Saleh M., 2020: Impact of Lithofacies and Structures on the Hydrogeochemistry of the Lower Miocene Aquifer at Moghra Oasis, NorthWestern Desert, Egypt. *Nat. Resour. Res.*, **29**, 6, 3789–3817, doi: 10.1007/s11053-020-09679-3.
- Abdel-Gawad A. M., El Abd E. A., Gedamy Y. R., 2020: Geological characteristics of shallow groundwater aquifer and its relation to hydrochemical features and bacteriological pollutants in Siwa Oasis, Egypt. *Int. J. Environ.*, **9**, 2, 117–147, doi: 10.36632/ije/2020.9.2.8.
- Abdel-Mogheeth S. M., 1996: Groundwater hazards in Siwa Oasis, Egypt. In: Proceedings of the UNESCO/NWRC/ACSAD Workshops on Wadi Hydrology and Groundwater Protection, Cairo, Egypt (3-6 June 1996), 113–118.
- Abdelrahman E. M., Abdelazeem M., Gobashy M., 2019: A minimization approach to depth and shape determination of mineralized zones from potential field data using the Nelder-Mead simplex algorithm. *Ore Geol. Rev.*, **114**, 103123, doi: 10.1016/j.oregeorev.2019.103123.
- Abdel Zaher M., Saibi H., Mansour K., Khalil A., Soliman M., 2018: Geothermal exploration using airborne gravity and magnetic data at Siwa Oasis, Western Desert,

- Egypt. Renew. Sustain. Energy Rev., **82**, 3, 3824–3832, doi: 10.1016/j.rser.2017.10.088.
- Abo EL-Fadl M. M., Wassel M. A., Sayed A. Z., Mahmod A. M., 2015: Hydrochemical Characteristics of Groundwater in Siwa Oasis, Egypt. Part I, Significance of the Situation Groundwater Resources and Future Outlook. *Int. J. Sci. Res.*, **4**, 10, 447–458.
- Abouelmagd A., Sultan M., Sturchio N. C., Soliman F., Rashed M., Ahmed M., Kehew A. E., Milewski A., Chouinard K., 2014: Paleoclimate record in the Nubian sandstone aquifer, Sinai Peninsula, Egypt. *Quat. Res.*, **81**, 1, 158–167, doi: 10.1016/j.yqres.2013.10.017.
- Aero-Service, 1984: Final operational report of airborne magnetic/radiation survey in the Eastern Desert, Egypt. Conducted for the Egyptian General Petroleum Corporation (EGPC) and the Egyptian Geological Survey and Mining Authority (EGSMA), Aero-Service Division, Houston, Texas, USA, Six Volumes.
- Affi A. H., 2005: Assessment of the hydrogeological conditions of groundwater in Siwa Oasis, North Western Desert, Egypt. Ph.D. Thesis, Minufiya Univ., Egypt, 98 p.
- Al-Garni M. A., El-Behiry M. G., Gobashy M. M., 2012: Geophysical survey for geological hazards assessment of Wadi Thuwal area, KSA: A case history. *Arab. J. Geosci.*, **5**, 1, 133–146, doi: 10.1007/s12517-010-0147-9.
- Al-Garni M. A., Gobashy M. M., 2010: Ground magnetic Investigation of subsurface structures Affecting Wadi Thuwal area, KSA. *J. King Abdulaziz Univ. Earth Sci.*, **21**, 2, 167–193, doi: 10.4197/ear.21-2.7.
- Al-Garni M., Hassanein H., Gobashy M., 2006: Geophysical investigation of groundwater in Wadi Lusab, Haddat Ash-Sham area, Makkah Al-Mukarramah. *Arab. Gulf J. Sci. Res.*, **24**, 2, 83–93.
- Aly A. A., 2001: Spatiotemporal monitoring and assessment of water resources in Siwa Oasis. M.Sc. Thesis, Faculty of Agriculture, Alexandria University, Alexandria, Egypt.
- Aly A. A., 2007: A holistic ecosystem approach for sustainable management of land and water resources in Siwa Oasis. Ph.D. Thesis, Faculty of Agriculture, Alexandria University, Alexandria, Egypt.
- Aly A. A., 2015: Hydrochemical characteristics of Egypt's western desert oases groundwater. *Arab. J. Geosci.*, **8**, 9, 7551–7564, doi: 10.1007/s12517-014-1680-8.
- Aly A. A., Gaber H. M., Kishk F. M., 2008: Long-term change detection and assessment of groundwater quality in Siwa Oasis. Egypt available water resources and future constrain conference, Geography and GIS Dept., Faculty of Arts, Alexandria University, Alexandria, Egypt, 17 July 2008, 19.
- Aly A. A., Abbas A. A., Benaabidate L., 2011: Hydrochemistry and quality of groundwater resources in Egypt: Case study of the Egyptian southern oases (Chapter 17). In: Scozzari A., El Mansouri B. (Eds.): Water security in the Mediterranean region, NATO Science for Peace and Security Series C: Environmental Security, Springer, Netherlands, 239–254, doi: 10.1007/978-94-007-1623-0\_17.

- Aly A. A., Kishk F. M., Gaber H. M., Al-Omran A. M., 2016: Long-term detection and hydrochemistry of groundwater resources in Egypt: A case study of Siwa Oasis. *J. Saudi Soc. Agric. Sci.*, **15**, 1, 67–74, doi: 10.1016/j.jssas.2014.04.003.
- Aly A. A., 2020: Soil and groundwater salinization in Siwa Oasis and management opportunities. Twenty-year change detection and assessment. *Arid Land Res. Manag.*, **34**, 2, 117–135, doi: 10.1080/15324982.2019.1635662.
- Antar M. S. M., 2011: Paleo-environments of the exposed Eocene Sediments between Wadi El-Hitan and east Siwa in the Egyptian Western Desert based on their faunal content especially the vertebrates. Ph.D. Thesis, Zagazig University, Faculty of Science, Geology Department, Egypt.
- Apaydin A., 2010: Relation of tectonic structure to groundwater flow in the Beypazari region, NW Anatolia, Turkey. *Hydrogeol. J.*, **18**, 6, 1343–1356, doi: 10.1007/s10040-010-0605-1.
- Araffa S. A. S., Gobashy M. M., Khalil M. H., Abdelaal A., 2021: Integration of geophysical techniques to detect geotechnical hazards: A case study in Mokattam, Cairo, Egypt. *Bull. Eng. Geol. Environ.*, **80**, 10, 8021–8041, doi: 10.1007/s10064-021-02388-y.
- Arnous M. O., El-Rayes A. E., Helmy A. M., 2017: Land-use/land-cover change: A key to understanding land degradation and relating environmental impacts in Northwestern Sinai, Egypt. *Environ. Earth Sci.*, **76**, 7, 263, doi: 10.1007/s12665-017-6571-3.
- Atchuta Rao D., Ram Babu H. V. Sanker Narayan P. V., 1981: Interpretation of magnetic anomalies due to dikes: The complex gradient method. *Geophysics*, **46**, 11, 1572–1578, doi: 10.1190/1.1441164.
- Attwa M., Gemal K. H., Eleraki M., 2016: Use of salinity and resistivity measurements to study the coastal aquifer salinization in a semi-arid region: A case study in northeast Nile Delta, Egypt. *Environ. Earth Sci.*, **75**, 9, 784, doi: 10.1007/s12665-016-5585-6.
- Awad M. A., Abdel Baki A. A., Hamza M. S., 1995: Isotope hydrology and geochemistry of water resources of Siwa Oasis, Western Desert, Egypt. Extended Synopses, Inter. Symposium on Isotopes in Water Resources Management, Austria (IAEA-SM-336/11p), 112–116.
- Azeem M. A., Mekkawi M., Gobashy M., 2014: Subsurface structures using a new integrated geophysical analysis, South Aswan, Egypt. *Arab. J. Geosci.*, **7**, 12, 5141–5157, doi: 10.1007/s12517-013-1140-x.
- Batayneh A. T., 2009: A hydrogeophysical model of the relationship between geoelectric and hydraulic parameters, central Jordan. *J. Water Resour. Prot.*, **1**, 6, 400–407, doi: 10.4236/jwarp.2009.16048.
- Campbell R. E., 1977: Geophysical drill hole casing anomalies. In: Workshop on Mining Geophysics, Univ. of Utah, Dept. Geol. Geophys, Report on NSF Grant AER76-80802, 257–268.
- Carrow R. N., Duncan R. R., 1998: Salt-Affected Turfgrass Sites: Assessment and Management. 1st ed., John Wiley & Sons, Chelsea (MI), Ann Arbor Press., 185 p.

- Chapman D., 1996: Water quality assessments: A guide to use of biota, sediments and water in environmental monitoring (2nd ed.). University Press, Cambridge, ISBN 0 419 21590 5 (HB).
- Conoco, 1987: Geologic map of Egypt. Egyptian general authority for petroleum (UN-ESCO Joint Map Project), 20 Sheets, Scale 1:500000, Cairo.
- Dahab K. A., 2004: Impact of the present groundwater exploitation system on the Nubia sandstone aquifer in Siwa Oasis, Western Desert, Egypt. In: 6th Intern. Conf. on Geochemistry, Alexandria Univ., Egypt, 5-16 Sept., 2004, 319–337.
- de Oliveira Braga A. C., Filho W. M., Dourado J. C., 2006: Resistivity (DC) method applied to aquifer protection studies. *Braz. J. Geophys.*, **24**, 4, 573–581.
- EGPC (Egyptian General Petroleum Corporation), 1989: Mineral, petroleum and groundwater assessment program. AID project, 263-0105 and amendment No. 1. Reduction to the pole magnetic anomaly map.
- EGPC (Egyptian General Petroleum Corporation), 1992: Western Desert, oil and gas fields (A comprehensive overview). EGPC, Cairo, Egypt, 431 p.
- Ehirim C. N., Nwankwo C. N., 2010: Evaluation of aquifer characteristics and groundwater quality using geoelectric method in Choba, Port Harcourt. *Arch. Appl. Sci. Res.*, **2**, 2, 396–403.
- El Arabi N., Idris Y., Fekry A., 2013: Temporal and spatial change detection of variations in the groundwater composition by multivariate statistical techniques. *N. Y. Sci. J.*, **6**, 11, 38–48.
- El Hossary M. F., 1999: Evaluation and management of groundwater resources in Siwa area with emphasis on the Nubian Sandstone aquifer. Ph.D. Thesis, Faculty of Science Ain Shams University, Egypt, 143 p.
- El Hossary M. F., 2013: Investigating the development challenges to Siwa Oasis, Northwestern Desert, Egypt. *N. Y. Sci. J.*, **6**, 4, 55–61.
- El Osta M., 2018: Maximizing the management of groundwater resources in the Paris–Abu Bayan reclaimed area, Western Desert, Egypt. *Arab. J. Geosci.*, **11**, 20, 642, doi: 10.1007/s12517-018-3945-0.
- El Osta M., Masoud M., Ezzeldin H., 2020: Assessment of the geochemical evolution of groundwater quality near the El Kharga Oasis, Egypt using NETPATH and water quality indices. *Environ. Earth Sci.*, **79**, 2, 56, doi: 10.1007/s12665-019-8793-z.
- El Osta M., Masoud M., Badran O., 2021: Aquifer hydraulic parameters estimation based on hydrogeophysical methods in West Nile Delta, Egypt. *Environ. Earth Sci.*, **80**, 9, 344, doi: 10.1007/s12665-021-09617-3.
- Elango L., Kannan R., 2007: Chapter 11 Rock–water interaction and its control on chemical composition of groundwater. In: Sarkar D., Datta R., Hannigan R. (Eds.): Concepts and Applications in Environmental Geochemistry, Developments in Environmental Science, **5**, 229–243, doi: 10.1016/S1474-8177(07)05011-5.
- El-Rayes A. E., Arnous M. O., Aziz A. M., 2017: Morphotectonic controls of groundwater flow regime and relating environmental impacts in Northwest Sinai, Egypt. *Arab. J. Geosci.*, **10**, 18, 401, doi: 10.1007/s12517-017-3188-5.

- El Shazly E. M., Abdel Hady M. A., El Ghawaby M. A., Khawasik S. M., El Shazly M. M., 1976: Geologic interpretation of LANDSAT satellite images for the Qatara Depression Area, Egypt. OSU-Remote Sensing Center, Academy of Scientific Research and Technology, Cairo.
- Farrag A. A., El Sayed E. A., Megahed H. A., 2016: Land use/land cover change detection and classification using remote sensing and GIS techniques: A case study at Siwa Oasis, Northwestern Desert of Egypt. *Cloud Publications, Int. J. Adv. Remote Sens. GIS*, **5**, 3, 1649–1661, Article ID Tech-558 ISSN 2320 – 0243.
- Farrag A. A., Sediek U. R., 2017: Evaluation hydrochemical analyses of groundwater and its suitability for drinking and agricultural uses at Western Desert of Egypt. Twentieth International Water Technology Conference, IWTC20, Hurgada, 18–20.
- Flathe H., 1955: Possibilities and limitations in applying geoelectrical methods to hydrogeological problems in the coastal area of northwest Germany. *Geophys. Prospect.*, **3**, 2, 95–110, doi: 10.1111/j.1365-2478.1955.tb01363.x.
- Flathe H., 1970: Interpretation of geoelectrical resistivity measurements for solving hydrogeological problems. In: Morley L. W. (Ed.): Mining and groundwater geophysics. Geological Survey of Canada, Economic Geology Report 26, 580–597.
- Flathe H., 1976: The role of geoelectric concept in geophysical research work for solving hydrological problems. *Geoexploration*, **14**, 3-4, 195–206, doi: 10.1016/0016-7142(76)90013-2.
- Gad M., Dahab K., Ibrahim H., 2018: Applying of a geochemical model on the Nubian sandstone aquifer in Siwa Oasis, Western Desert, Egypt. *Environ. Earth Sci.*, **77**, 11, 401, doi: 10.1007/s12665-018-7580-6.
- Gindy A. R., El Askary M. A., 1969: Stratigraphy, structure, and origin of Siwa depression, Western Desert of Egypt. *Am. Assoc. Pet. Geol. Bull.*, **53**, 3, 603–625, doi: 10.1306/5d25c6a1-16c1-11d7-8645000102c1865d.
- Gobashy M. M., Al-Garni M. A., 2008: High resolution ground magnetic survey (HRGM) for determining the optimum location of Subsurface Dam in Wadi Nu'man, Makkah Al Mukarammah, KSA. *J. King Abdulaziz Univ. Earth Sci.*, **19**, 1, 57–83, doi: 10.4197/ear.19-1.4.
- Gobashy M., Abdelazeem M., Abdrabou M., 2020: Minerals and ore deposits exploration using meta-heuristic based optimization on magnetic data. *Contrib. Geophys. Geod.*, **50**, 2, 161–199, doi: 10.31577/congeo.2020.50.2.1.
- Gobashy M. M., Eldougdoug A., Abdelazeem M., Abdelhalim A., 2021a: Future development of gold mineralization utilizing remote sensing and aeromagnetic techniques: A case study, Barramiya mining district, Central Eastern Desert of Egypt. *Nat. Resour. Res.*, **30**, 3, 2007–2028, doi: 10.1007/s11053-021-09824-6.
- Gobashy M. M., Metwally A. M., Abdelazeem M., Soliman K. S., Abdelhalim A., 2021b: Geophysical Exploration of Shallow Groundwater Aquifers in Arid Regions: A Case Study of Siwa Oasis, Egypt. *Nat. Resour. Res.*, **30**, 5, 3355–3384, doi: 10.1007/s11053-021-09897-3.
- Gobashy M. M., Abbas E. A. S., Soliman K. S., Abdelhalim A., 2022: Mapping of gold mineralization using an integrated interpretation of geological and geophysical

- data—a case study from West Baranes, South Eastern Desert, Egypt. *Arab. J. Geosci.*, **15**, 22, 1692, doi: 10.1007/s12517-022-10955-0.
- GPC (General Petroleum Company), 1991: Salinity study on Pre-Upper Cenomanian (PUC) sediments in Siwa area. Internal technical report in the General Petroleum Company, Nasr City, Cairo.
- Hedia R. M. R., 2015: Assessment of drainage water quality in Siwa Oasis and its suitability for reuse in agricultural irrigation. *Egypt. J. Soil Sci.*, **55**, 4, 501–515, doi: 10.21608/EJSS.2015.1568.
- Hem J. D., 1970: Study and interpretation of chemical characteristics of natural water, 2nd ed. U.S. Geological Survey, Geological Survey water supply paper 1473, U.S. Government Printing Office, Washington, 363 p.
- Henriet J. P., 1976: Direct application of the Dar Zarrouk parameters in groundwater surveys. *Geophys. Prospect.*, **24**, 2, 344–353, doi: 10.1111/j.1365-2478.1976.tb00931.x.
- Herrera E., Garfias J., 2013: Characterizing a fractured aquifer in Mexico using geological attributes related to open pit groundwater. *Hydrogeol. J.*, **21**, 6, 1323–1338, doi: 10.1007/s10040-013-0992-1.
- Himida I. H., 1970: The Nubian Artesian basin its regional hydrogeological aspects and paleohydrogeological reconstruction. *J. Hydrol.: N. Z.*, **9**, 2, 89–116.
- Hsu S.-K., Sibuet J.-C., Shyu C.-T., 1996: High-resolution detection of geologic boundaries from potential-field anomalies: An enhanced analytic signal technique. *Geophysics*, **61**, 2, 373–386, doi: 10.1190/1.1443966.
- Ibrahim S. A., 1991: Studies on groundwater possibilities in the northern part of the Western Desert–Egypt. Ph.D. Thesis, Cairo University, Cairo, Egypt, 292 p.
- IPI2Win-1D Program, 2000: Programs set for 1-D VES data interpretation. Dept. of Geophysics, Geological Faculty, Moscow University, Russia.
- Iyasele J. U., David J., Idiata D. J., 2015: Investigation of the relationship between electrical conductivity and total dissolved solids for mono-valent, di-valent, and trivalent metal compounds. *Int. J. Eng. Res. Rev.*, **3**, 1, 40–48.
- Jagadeeswara Rao P., Suryaprakasa Rao B., Jagannadha Rao M., Harikrishna P., 2003: Geo-electrical data analysis to demarcate groundwater pockets and recharge zones in Champavathi River Basin, Vizianagaram District, Andhra Pradesh. *J. Indian Geophys. Union*, **7**, 2, 105–113.
- Kaiser C. P., Vollen Weider F. W., 1972: WEPCO Oil and Gas prospects of Western Desert and Nile Delta. Unpublished report, WEPCO.
- Keller G. V., Frischknecht F. C., 1966: Electrical methods in geophysical prospecting. Pergamon Press, New York, 179–187.
- Khalil A., Abd El All E., Rabeh T., Osman S., 2015: Integrated geophysical study to delineate the subsurface structures in Siwa Oasis, Western Desert, Egypt. *Geophys. Res. Abstr.*, **17**, EGU General Assembly, 12–17 April, 2015, Vienna, Austria, id. 91.
- Kumar M. S., Gnanasundar D., Elango L., 2001: Geophysical studies to determine hydraulic characteristics of an alluvial aquifer. *J. Environ. Hydrol.*, **9**, 15, 1–8.

- Maillet R., 1947: The fundamental equations of electrical prospecting. *Geophysics*, **12**, 4, 529–556, doi: 10.1190/1.1437342.
- Manning A. H., 2011: Mountain-block recharge, present, and past, in the eastern Española Basin, New Mexico, USA. *Hydrogeol. J.*, **19**, 2, 379–397, doi: 10.1007/s10040-010-0696-8.
- Marsden D., 1973: The automatic fitting of a resistivity sounding by a geometrical progression of depths. *Geophys. Prospect.*, **21**, 2, 266–280, doi: 10.1111/j.1365-2478.1973.tb00027.x.
- Masoud M., 2020: Groundwater resources management of the shallow groundwater aquifer in the Desert Fringes of El Beheira Governorate, Egypt. *Earth Syst. Environ.*, **4**, 1, 147–165, doi: 10.1007/s41748-020-00148-8.
- Mazáč O., Kelly W. E., Landa I., 1985: A hydrogeophysical model for relations between electrical and hydraulic properties of aquifers. *J. Hydrol.*, **79**, 1-2, 1–19, doi: 10.1016/0022-1694(85)90178-7.
- Moghazy N. H., Kaluarachchi J. J., 2020: Assessment of groundwater resources in Siwa Oasis, Western Desert, Egypt. *Alex. Eng. J.*, **59**, 1, 149–163, doi: 10.1016/j.aej.2019.12.018.
- Mooney H. M., Orellana E., Pickett H., Tornheim L., 1966: A resistivity computation method for layered earth models. *Geophysics*, **31**, 1, 192–203, doi: 10.1190/1.1439733.
- Nabighian M. N., 1972: The analytic signal of two-dimensional magnetic bodies with polygonal cross-section: Its properties, and use for automated anomaly interpretation. *Geophysics*, **37**, 3, 507–517, doi: 10.1190/1.1440276.
- Nabighian M. N., 1974: Additional comments on the analytic signal of two-dimensional magnetic bodies with polygonal cross-section. *Geophysics*, **39**, 1, 85–92, doi: 10.1190/1.1440416.
- Nabighian M. N., 1984: Toward a three-dimensional automatic interpretation of potential field data via generalized Hilbert transform: Fundamental relations. *Geophysics*, **49**, 6, 780–786, doi: 10.1190/1.1441706.
- Nazih M., Gobashy M. M., Salem Z., Soliman K. S., Hassan A. A. M., 2022: Hydro-geochemical and geophysical investigations to delineate underground water aquifer in arid regions: A case study, Gara oasis, Egypt. *Contrib. Geophys. Geod.*, **52**, 3, 307–357. doi: 10.31577/congeo.2022.52.3.1.
- Niwas S., Singhal D. C., 1981: Estimation of aquifer transmissivity from Dar-Zarrouk parameters in porous media. *J. Hydrol.*, **50**, 393–399, doi: 10.1016/0022-1694(81)90082-2.
- Nwankwo C., Nwosu L., Emujakporue G., 2011: Determination of Dar Zarouk parameters for the assessment of groundwater resources potential: Case study of Imo State, southeastern Nigeria. *J. Econ. Sustain. Dev.*, **2**, 8, 57–71.
- Ogilvy A. A., 1970: Geophysical prospecting for groundwater in the Soviet Union. In: Morley L. W. (Ed.): *Mining and groundwater geophysics*. Geological Survey of Canada, Economic Geology Report 26, 536–543.
- Orellana E., 1963: Properties and drawings of the so-called Dar Zarrouk curves. *Geophysics*, **28**, 1, 99–110, doi: 10.1190/1.1439158.

- Oteri A. U., 1981: Geoelectric investigation of saline contamination of chalk aquifer by mine drainage water at Tilmanstone, England. *Geoexploration*, **19**, 3, 179–192, doi: 10.1016/0016-7142(81)90002-8.
- Patella D., 1975: A numerical computation procedure for the direct interpretation of geoelectrical soundings. *Geophys. Prospect.*, **23**, 2, 335–362, doi: 10.1111/j.1365-2478.1975.tb01533.x.
- Portniaguine O., Zhdanov M. S., 1999: Focusing geophysical inversion images. *Geophysics*, **64**, 3, 874–887, doi: 10.1190/1.1444596.
- Rabeh T., 2004: Evaluation of subsurface structures of Siwa oasis, western Desert, Egypt using 3-D magnetic modeling. *Egypt. Geol. Surv. J.*, **33**, 224–260.
- Rehman F., Abdelazeem M., Gobashy M. M., Harby H. M., Rehman F., Abuelnaga H. S. O., 2019: Application of magnetic method to define the structural setting controlling the contaminated area of Wadi Bani Malik, east Jeddah, Saudi Arabia. *Boll. Geofis. Teor. Appl.*, **60**, 1, 97–122, doi: 10.4430/bgta0269.
- Reynolds J. M., 1997: An introduction to applied and environmental geophysics. John Wiley & Sons Ltd., 796 p.
- Roest W. R., Verhoef J., Pilkington M., 1992: Magnetic interpretation using the 3-D analytic signal. *Geophysics*, **57**, 1, 116–125, doi: 10.1190/1.1443174.
- Roques C., Bour O., Aquilina L., Dewandel B., Leray S., Schroetter J. M., Longueuevigne L., Le Borgne T., Hochreutener R., Labasque T., Lavenant N. Vergnaud-Ayraud V., Mougin B., 2014: Hydrological behavior of a deep sub-vertical fault in crystalline basement and relationships with surrounding reservoirs. *J. Hydrol.*, **509**, 42–54, doi: 10.1016/j.jhydrol.2013.11.023.
- Roy K. K., Elliot H. M., 1981: Some observation regarding depth of exploration in D.C. electrical methods. *Geoexploration*, **19**, 1, 1–13, doi: 10.1016/0016-7142(81)90009-0.
- Said R., 1962: *The Geology of Egypt*. Elsevier Publ. Co., Amsterdam, Holland.
- Said R., 1990: *The Geology of Egypt*. Elsevier Publ. Co., Amsterdam and New York.
- Saleh I. H., Elnaggar A. M., Ibrahim H. Z., 2016: Risk assessment of radionuclides in groundwater in Siwa Oasis, Egypt. *Int. J. Adv. Res.*, **4**, 11, 1459–1466, doi: 10.21474/IJAR01/2233.
- Salem A., Williams S., Fairhead D., Smith R., Ravat D., 2008: Interpretation of magnetic data using tilt-angle derivatives. *Geophysics*, **73**, 1, L1–L10, doi: 10.1190/1.2799992.
- Salheen M. A., 2013: Towards a water-based regional development model for Siwa oasis in the Western Desert-Egypt. GCCBS 2013 conference program.
- Salman S. A., Abu El Ella E. M., Seleem E. M., Elnazer A. A., 2018: Groundwater quality and environmental investigations in Siwa Oasis, Egypt. *Int. J. Recent Adv. Multidiscip. Res.*, **5**, 7, 3951–3958.
- Shata A. A., 1982: Hydrogeology of the great Nubia sandstone basin, Egypt. *Q. J. Eng. Geol. Hydrogeol.*, **15**, 2, 127–133, doi: 10.1144/GSL.QJEG.1982.015.02.04.
- Singh K. P., 2005: Nonlinear estimation of aquifer parameters from surficial resistivity measurements. *Hydrol. Earth Sys. Sci. Discuss.*, **2**, 917–938.

- Singh U. K., Das R. K., Hodlur G. K., 2004: Significance of Dar-Zarrouk parameters in the exploration of quality-affected coastal aquifer systems. *Environ. Geol.*, **45**, 5, 696–702, doi: 10.1007/s00254-003-0925-8.
- Srinivas Y., Hudson Oliver D., Stanley Raj A., Muthuraj D., Chandrasekar N., 2012: Estimation of conductance anomalies in subsurface through Dar-Zarrouk parameters by resistivity inversion method. *Int. J. Phys. Math. Sci.*, **3**, 1, 140–151.
- Utom A. U., Odoh B. I., Okoro A. U., 2012: Estimation of aquifer transmissivity using Dar Zarrouk parameters derived from surface resistivity measurements: A case history from parts of Enugu Town (Nigeria). *J. Water Resour. Prot.*, **4**, 12, 993–1000, doi: 10.4236/jwarp.2012.412115.
- Van Der Velpen B. P. A., 1988: Computer Program RESIST, version 1.0a package for the processing of the resistivity sounding data. M.Sc. Research Project. ITC, Delft, the Netherlands.
- Worthington P. F., 1975: Quantitative geophysical investigations of granular aquifers. *Surv. Geophys.*, **2**, 3, 313–366, doi: 10.1007/BF01447858.
- Youssef M. I., 1968: Structural pattern of Egypt and its interpretation. *Am. Assoc. Pet. Geol. Bull.*, **52**, 4, 601–614, doi: 10.1306/5D25C44D-16C1-11D7-8645000102C1865D.
- Yuan R., Song X., Zhang Y., Han D., Wang S., Tang C., 2011: Using major ions and stable isotopes to characterize recharge regime of a fault-influenced aquifer in Beiyishui River Watershed, North China plain. *J. Hydrol.*, **405**, 3-4, 512–521, doi: 10.1016/j.jhydrol.2011.05.048.
- Zohdy A. A. R., 1965: The auxiliary point method of electrical sounding interpretation, and its relationship to the Dar Aarrouk parameters. *Geophysics*, **30**, 4, 644–660, doi: 10.1190/1.1439636.
- Zohdy A. A. R., Eaton G. P., Mabey D. R., 1974: Application of surface geophysics to groundwater investigations: techniques of water resources investigation. U.S. Geological Survey Book 2, Chapter D1, US Government Printing Office, Washington, 116.
- Zohdy A. A. R., 1989: A new method for automatic interpretation of Schlumberger and Wenner sounding curves. *Geophysics*, **54**, 2, 245–253, doi: 10.1190/1.1442648.